UC Berkeley
UC Berkeley Previously Published Works

Title
Measurement of branching fractions of B decays to K1(1270)π and K1(1400)π and determination of the CKM angle α from B0→a1(1260)±π∓

Permalink
https://escholarship.org/uc/item/0fm3z82q

Journal
Physical Review D, 81(5)

ISSN
2470-0010

Authors
Aubert, B
Karyotakis, Y
Lees, JP
et al.

Publication Date
2010-03-01

DOI
10.1103/physrevd.81.052009

Copyright Information
This work is made available under the terms of a Creative Commons Attribution License, availalbe at https://creativecommons.org/licenses/by/4.0/

Peer reviewed

Measurement of branching fractions of B decays to $K_1(1270)\pi$ and $K_1(1400)\pi$ and determination of the CKM angle α from $B^0 \to a_1(1260)^{\pm}\pi^{\mp}$

B. Aubert,[1] Y. Karyotakis,[1] J. P. Lees,[1] V. Poireau,[1] E. Prencipe,[1] X. Prudent,[1] V. Tisserand,[1] J. Garra Tico,[2] E. Grauges,[2] M. Martinelli,[3a,3b] A. Palano,[3a,3b] M. Pappagallo,[3a,3b] G. Eigen,[4] B. Stugu,[4] L. Sun,[4] M. Battaglia,[5] D. N. Brown,[5] B. Hooberman,[5] L. T. Kerth,[5] Yu. G. Kolomensky,[5] G. Lynch,[5] I. L. Osipenkov,[5] K. Tackmann,[5] T. Tanabe,[5] C. M. Hawkes,[6] N. Soni,[6] A. T. Watson,[6] H. Koch,[7] T. Schroeder,[7] D. J. Asgeirsson,[8] C. Hearty,[8] T. S. Mattison,[8] J. A. McKenna,[8] M. Barrett,[9] A. Khan,[9] A. Randle-Conde,[9] V. E. Blinov,[10] A. D. Bukin,[10,*] A. R. Buzykaev,[10] V. P. Druzhinin,[10] V. B. Golubev,[10] A. P. Onuchin,[10] S. I. Serednyakov,[10] Yu. I. Skovpen,[10] E. P. Solodov,[10] K. Yu. Todyshev,[10] M. Bondioli,[11] S. Curry,[11] I. Eschrich,[11] D. Kirkby,[11] A. J. Lankford,[11] P. Lund,[11] M. Mandelkern,[11] E. C. Martin,[11] D. P. Stoker,[11] H. Atmacan,[12] J. W. Gary,[12] F. Liu,[12] O. Long,[12] G. M. Vitug,[12] Z. Yasin,[12] V. Sharma,[13] C. Campagnari,[14] T. M. Hong,[14] D. Kovalskyi,[14] M. A. Mazur,[14] J. D. Richman,[14] T. W. Beck,[15] A. M. Eisner,[15] C. A. Heusch,[15] J. Kroseberg,[15] W. S. Lockman,[15] A. J. Martinez,[15] T. Schalk,[15] B. A. Schumm,[15] A. Seiden,[15] L. Wang,[15] L. O. Winstrom,[15] C. H. Cheng,[16] D. A. Doll,[16] B. Echenard,[16] F. Fang,[16] D. G. Hitlin,[16] I. Narsky,[16] P. Ongmongkolkul,[16] T. Piatenko,[16] F. C. Porter,[16] R. Andreassen,[17] G. Mancinelli,[17] B. T. Meadows,[17] K. Mishra,[17] M. D. Sokoloff,[17] P. C. Bloom,[18] W. T. Ford,[18] A. Gaz,[18] J. F. Hirschauer,[18] M. Nagel,[18] U. Nauenberg,[18] J. G. Smith,[18] S. R. Wagner,[18] R. Ayad,[19,†] W. H. Toki,[19] R. J. Wilson,[19] E. Feltresi,[20] A. Hauke,[20] H. Jasper,[20] T. M. Karbach,[20] J. Merkel,[20] A. Petzold,[20] B. Spaan,[20] K. Wacker,[20] M. J. Kobel,[21] R. Nogowski,[21] K. R. Schubert,[21] R. Schwierz,[21] D. Bernard,[22] E. Latour,[22] M. Verderi,[22] P. J. Clark,[23] S. Playfer,[23] J. E. Watson,[23] M. Andreotti,[24a,24b] D. Bettoni,[24a] C. Bozzi,[24a] R. Calabrese,[24a,24b] A. Cecchi,[24a,24b] G. Cibinetto,[24a,24b] E. Fioravanti,[24a,24b] P. Franchini,[24a,24b] E. Luppi,[24a,24b] M. Munerato,[24a,24b] M. Negrini,[24a,24b] A. Petrella,[24a,24b] L. Piemontese,[24a] V. Santoro,[24a,24b] R. Baldini-Ferroli,[25] A. Calcaterra,[25] R. de Sangro,[25] G. Finocchiaro,[25] S. Pacetti,[25] P. Patteri,[25] I. M. Peruzzi,[25,‡] M. Piccolo,[25] M. Rama,[25] A. Zallo,[25] R. Contri,[26a,26b] E. Guido,[26a,26b] M. Lo Vetere,[26a,26b] M. R. Monge,[26a,26b] S. Passaggio,[26a] C. Patrignani,[26a,26b] E. Robutti,[26a] S. Tosi,[26a,26b] K. S. Chaisanguanthum,[27] M. Morii,[27] A. Adametz,[28] J. Marks,[28] S. Schenk,[28] U. Uwer,[28] F. U. Bernlochner,[29] V. Klose,[29] H. M. Lacker,[29] T. Lueck,[29] A. Volk,[29] D. J. Bard,[30] P. D. Dauncey,[30] M. Tibbetts,[30] P. K. Behera,[31] M. J. Charles,[31] U. Mallik,[31] J. Cochran,[32] H. B. Crawley,[32] L. Dong,[32] V. Eyges,[32] W. T. Meyer,[32] S. Prell,[32] E. I. Rosenberg,[32] A. E. Rubin,[32] Y. Y. Gao,[33] A. V. Gritsan,[33] Z. J. Guo,[33] N. Arnaud,[34] J. Béquilleux,[34] A. D'Orazio,[34] M. Davier,[34] D. Derkach,[34] J. Firmino da Costa,[34] G. Grosdidier,[34] F. Le Diberder,[34] V. Lepeltier,[34] A. M. Lutz,[34] B. Malaescu,[34] S. Pruvot,[34] P. Roudeau,[34] M. H. Schune,[34] J. Serrano,[34] V. Sordini,[34,§] A. Stocchi,[34] G. Wormser,[34] D. J. Lange,[35] D. M. Wright,[35] I. Bingham,[36] J. P. Burke,[36] C. A. Chavez,[36] J. R. Fry,[36] E. Gabathuler,[36] R. Gamet,[36] D. E. Hutchcroft,[36] D. J. Payne,[36] C. Touramanis,[36] A. J. Bevan,[37] C. K. Clarke,[37] F. Di Lodovico,[37] R. Sacco,[37] M. Sigamani,[37] G. Cowan,[38] S. Paramesvaran,[38] A. C. Wren,[38] D. N. Brown,[39] C. L. Davis,[39] A. G. Denig,[40] M. Fritsch,[40] W. Gradl,[40] A. Hafner,[40] K. E. Alwyn,[41] D. Bailey,[41] R. J. Barlow,[41] G. Jackson,[41] G. D. Lafferty,[41] T. J. West,[41] J. I. Yi,[41] J. Anderson,[42] C. Chen,[42] A. Jawahery,[42] D. A. Roberts,[42] G. Simi,[42] J. M. Tuggle,[42] C. Dallapiccola,[43] E. Salvati,[43] R. Cowan,[44] D. Dujmic,[44] P. H. Fisher,[44] S. W. Henderson,[44] G. Sciolla,[44] M. Spitznagel,[44] R. K. Yamamoto,[44] M. Zhao,[44] P. M. Patel,[45] S. H. Robertson,[45] M. Schram,[45] P. Biassoni,[46a,46b] A. Lazzaro,[46a,46b] V. Lombardo,[46a] F. Palombo,[46a,46b] S. Stracka,[46a,46b] L. Cremaldi,[47] R. Godang,[47,‖] R. Kroeger,[47] P. Sonnek,[47] D. J. Summers,[47] H. W. Zhao,[47] M. Simard,[48] P. Taras,[48] H. Nicholson,[49] G. De Nardo,[50a,50b] L. Lista,[50a] D. Monorchio,[50a,50b] G. Onorato,[50a,50b] C. Sciacca,[50a,50b] G. Raven,[51] H. L. Snoek,[51] C. P. Jessop,[52] K. J. Knoepfel,[52] J. M. LoSecco,[52] W. F. Wang,[52] L. A. Corwin,[53] K. Honscheid,[53] H. Kagan,[53] R. Kass,[53] J. P. Morris,[53] A. M. Rahimi,[53] S. J. Sekula,[53] Q. K. Wong,[53] N. L. Blount,[54] J. Brau,[54] R. Frey,[54] O. Igonkina,[54] J. A. Kolb,[54] M. Lu,[54] R. Rahmat,[54] N. B. Sinev,[54] D. Strom,[54] J. Strube,[54] E. Torrence,[54] G. Castelli,[55a,55b] N. Gagliardi,[55a,55b] M. Margoni,[55a,55b] M. Morandin,[55a] M. Posocco,[55a] M. Rotondo,[55a] F. Simonetto,[55a,55b] R. Stroili,[55a,55b] C. Voci,[55a,55b] P. del Amo Sanchez,[56] E. Ben-Haim,[56] G. R. Bonneaud,[56] H. Briand,[56] J. Chauveau,[56] O. Hamon,[56] Ph. Leruste,[56] G. Marchiori,[56] J. Ocariz,[56] A. Perez,[56] J. Prendki,[56] S. Sitt,[56] L. Gladney,[57] M. Biasini,[58a,58b] E. Manoni,[58a,58b] C. Angelini,[59a,59b] G. Batignani,[59a,59b] S. Bettarini,[59a,59b] G. Calderini,[59a,59b,¶] M. Carpinelli,[59a,59b,**] A. Cervelli,[59a,59b] F. Forti,[59a,59b] M. A. Giorgi,[59a,59b] A. Lusiani,[59a,59c] M. Morganti,[59a,59b] N. Neri,[59a,59b] E. Paoloni,[59a,59b] G. Rizzo,[59a,59b] J. J. Walsh,[59a] D. Lopes Pegna,[60] C. Lu,[60] J. Olsen,[60] A. J. S. Smith,[60] A. V. Telnov,[60] F. Anulli,[61a] E. Baracchini,[61a,61b] G. Cavoto,[61a] R. Faccini,[61a,61b] F. Ferrarotto,[61a] F. Ferroni,[61a,61b] M. Gaspero,[61a,61b] P. D. Jackson,[61a] L. Li Gioi,[61a] M. A. Mazzoni,[61a] S. Morganti,[61a] G. Piredda,[61a] F. Renga,[61a,61b] C. Voena,[61a] M. Ebert,[62] T. Hartmann,[62] H. Schröder,[62] R. Waldi,[62] T. Adye,[63] B. Franek,[63] E. O. Olaiya,[63] F. F. Wilson,[63] S. Emery,[64] L. Esteve,[64] G. Hamel de Monchenault,[64] W. Kozanecki,[64] G. Vasseur,[64]

Ch. Yèche,[64] M. Zito,[64] M. T. Allen,[65] D. Aston,[65] R. Bartoldus,[65] J. F. Benitez,[65] R. Cenci,[65] J. P. Coleman,[65]
M. R. Convery,[65] J. C. Dingfelder,[65] J. Dorfan,[65] G. P. Dubois-Felsmann,[65] W. Dunwoodie,[65] R. C. Field,[65]
M. Franco Sevilla,[65] B. G. Fulsom,[65] A. M. Gabareen,[65] M. T. Graham,[65] P. Grenier,[65] C. Hast,[65] W. R. Innes,[65]
J. Kaminski,[65] M. H. Kelsey,[65] H. Kim,[65] P. Kim,[65] M. L. Kocian,[65] D. W. G. S. Leith,[65] S. Li,[65] B. Lindquist,[65] S. Luitz,[65]
V. Luth,[65] H. L. Lynch,[65] D. B. MacFarlane,[65] H. Marsiske,[65] R. Messner,[65,*] D. R. Muller,[65] H. Neal,[65] S. Nelson,[65]
C. P. O'Grady,[65] I. Ofte,[65] M. Perl,[65] B. N. Ratcliff,[65] A. Roodman,[65] A. A. Salnikov,[65] R. H. Schindler,[65] J. Schwiening,[65]
A. Snyder,[65] D. Su,[65] M. K. Sullivan,[65] K. Suzuki,[65] S. K. Swain,[65] J. M. Thompson,[65] J. Va'vra,[65] A. P. Wagner,[65]
M. Weaver,[65] C. A. West,[65] W. J. Wisniewski,[65] M. Wittgen,[65] D. H. Wright,[65] H. W. Wulsin,[65] A. K. Yarritu,[65]
C. C. Young,[65] V. Ziegler,[65] X. R. Chen,[66] H. Liu,[66] W. Park,[66] M. V. Purohit,[66] R. M. White,[66] J. R. Wilson,[66] M. Bellis,[67]
P. R. Burchat,[67] A. J. Edwards,[67] T. S. Miyashita,[67] S. Ahmed,[68] M. S. Alam,[68] J. A. Ernst,[68] B. Pan,[68] M. A. Saeed,[68]
S. B. Zain,[68] A. Soffer,[69] S. M. Spanier,[70] B. J. Wogsland,[70] R. Eckmann,[71] J. L. Ritchie,[71] A. M. Ruland,[71]
C. J. Schilling,[71] R. F. Schwitters,[71] B. C. Wray,[71] B. W. Drummond,[72] J. M. Izen,[72] X. C. Lou,[72] F. Bianchi,[73a,73b]
D. Gamba,[73a,73b] M. Pelliccioni,[73a,73b] M. Bomben,[74a,74b] L. Bosisio,[74a,74b] C. Cartaro,[74a,74b] G. Della Ricca,[74a,74b]
L. Lanceri,[74a,74b] L. Vitale,[74a,74b] V. Azzolini,[75] N. Lopez-March,[75] F. Martinez-Vidal,[75] D. A. Milanes,[75] A. Oyanguren,[75]
J. Albert,[76] Sw. Banerjee,[76] B. Bhuyan,[76] H. H. F. Choi,[76] K. Hamano,[76] G. J. King,[76] R. Kowalewski,[76] M. J. Lewczuk,[76]
I. M. Nugent,[76] J. M. Roney,[76] R. J. Sobie,[76] T. J. Gershon,[77] P. F. Harrison,[77] J. Ilic,[77] T. E. Latham,[77]
G. B. Mohanty,[77] E. M. T. Puccio,[77] H. R. Band,[78] X. Chen,[78] S. Dasu,[78] K. T. Flood,[78] Y. Pan,[78] R. Prepost,[78]
C. O. Vuosalo,[78] and S. L. Wu[78]

(*BABAR* Collaboration)

[1]*Laboratoire d'Annecy-le-Vieux de Physique des Particules (LAPP), Université de Savoie,
CNRS/IN2P3, F-74941 Annecy-Le-Vieux, France*
[2]*Universitat de Barcelona, Facultat de Fisica, Departament ECM, E-08028 Barcelona, Spain*
[3a]*INFN Sezione di Bari, I-70126 Bari, Italy*
[3b]*Dipartimento di Fisica, Università di Bari, I-70126 Bari, Italy*
[4]*University of Bergen, Institute of Physics, N-5007 Bergen, Norway*
[5]*Lawrence Berkeley National Laboratory and University of California, Berkeley, California 94720, USA*
[6]*University of Birmingham, Birmingham, B15 2TT, United Kingdom*
[7]*Ruhr Universität Bochum, Institut für Experimentalphysik 1, D-44780 Bochum, Germany*
[8]*University of British Columbia, Vancouver, British Columbia, Canada V6T 1Z1*
[9]*Brunel University, Uxbridge, Middlesex UB8 3PH, United Kingdom*
[10]*Budker Institute of Nuclear Physics, Novosibirsk 630090, Russia*
[11]*University of California at Irvine, Irvine, California 92697, USA*
[12]*University of California at Riverside, Riverside, California 92521, USA*
[13]*University of California at San Diego, La Jolla, California 92093, USA*
[14]*University of California at Santa Barbara, Santa Barbara, California 93106, USA*
[15]*University of California at Santa Cruz, Institute for Particle Physics, Santa Cruz, California 95064, USA*
[16]*California Institute of Technology, Pasadena, California 91125, USA*
[17]*University of Cincinnati, Cincinnati, Ohio 45221, USA*
[18]*University of Colorado, Boulder, Colorado 80309, USA*
[19]*Colorado State University, Fort Collins, Colorado 80523, USA*
[20]*Technische Universität Dortmund, Fakultät Physik, D-44221 Dortmund, Germany*
[21]*Technische Universität Dresden, Institut für Kern- und Teilchenphysik, D-01062 Dresden, Germany*
[22]*Laboratoire Leprince-Ringuet, CNRS/IN2P3, Ecole Polytechnique, F-91128 Palaiseau, France*
[23]*University of Edinburgh, Edinburgh EH9 3JZ, United Kingdom*
[24a]*INFN Sezione di Ferrara, I-44100 Ferrara, Italy*
[24b]*Dipartimento di Fisica, Università di Ferrara, I-44100 Ferrara, Italy*
[25]*INFN Laboratori Nazionali di Frascati, I-00044 Frascati, Italy*
[26a]*INFN Sezione di Genova, I-16146 Genova, Italy*
[26b]*Dipartimento di Fisica, Università di Genova, I-16146 Genova, Italy*
[27]*Harvard University, Cambridge, Massachusetts 02138, USA*
[28]*Universität Heidelberg, Physikalisches Institut, Philosophenweg 12, D-69120 Heidelberg, Germany*
[29]*Humboldt-Universität zu Berlin, Institut für Physik, Newtonstrasse 15, D-12489 Berlin, Germany*
[30]*Imperial College London, London, SW7 2AZ, United Kingdom*
[31]*University of Iowa, Iowa City, Iowa 52242, USA*
[32]*Iowa State University, Ames, Iowa 50011-3160, USA*

[33]Johns Hopkins University, Baltimore, Maryland 21218, USA

[34]Laboratoire de l'Accélérateur Linéaire, IN2P3/CNRS et Université Paris-Sud 11,
Centre Scientifique d'Orsay, B. P. 34, F-91898 Orsay Cedex, France

[35]Lawrence Livermore National Laboratory, Livermore, California 94550, USA

[36]University of Liverpool, Liverpool L69 7ZE, United Kingdom

[37]Queen Mary, University of London, London, E1 4NS, United Kingdom

[38]University of London, Royal Holloway and Bedford New College, Egham, Surrey TW20 0EX, United Kingdom

[39]University of Louisville, Louisville, Kentucky 40292, USA

[40]Johannes Gutenberg-Universität Mainz, Institut für Kernphysik, D-55099 Mainz, Germany

[41]University of Manchester, Manchester M13 9PL, United Kingdom

[42]University of Maryland, College Park, Maryland 20742, USA

[43]University of Massachusetts, Amherst, Massachusetts 01003, USA

[44]Massachusetts Institute of Technology, Laboratory for Nuclear Science, Cambridge, Massachusetts 02139, USA

[45]McGill University, Montréal, Québec, Canada H3A 2T8

[46a]INFN Sezione di Milano, I-20133 Milano, Italy

[46b]Dipartimento di Fisica, Università di Milano, I-20133 Milano, Italy

[47]University of Mississippi, University, Mississippi 38677, USA

[48]Université de Montréal, Physique des Particules, Montréal, Québec, Canada H3C 3J7

[49]Mount Holyoke College, South Hadley, Massachusetts 01075, USA

[50a]INFN Sezione di Napoli, I-80126 Napoli, Italy

[50b]Dipartimento di Scienze Fisiche, Università di Napoli Federico II, I-80126 Napoli, Italy

[51]NIKHEF, National Institute for Nuclear Physics and High Energy Physics, NL-1009 DB Amsterdam, The Netherlands

[52]University of Notre Dame, Notre Dame, Indiana 46556, USA

[53]Ohio State University, Columbus, Ohio 43210, USA

[54]University of Oregon, Eugene, Oregon 97403, USA

[55a]INFN Sezione di Padova, I-35131 Padova, Italy

[55b]Dipartimento di Fisica, Università di Padova, I-35131 Padova, Italy

[56]Laboratoire de Physique Nucléaire et de Hautes Energies, IN2P3/CNRS, Université Pierre et Marie Curie-Paris6,
Université Denis Diderot-Paris7, F-75252 Paris, France

[57]University of Pennsylvania, Philadelphia, Pennsylvania 19104, USA

[58a]INFN Sezione di Perugia, I-06100 Perugia, Italy

[58b]Dipartimento di Fisica, Università di Perugia, I-06100 Perugia, Italy

[59a]INFN Sezione di Pisa, I-56127 Pisa, Italy

[59b]Dipartimento di Fisica, Università di Pisa, I-56127 Pisa, Italy

[59c]Scuola Normale Superiore di Pisa, I-56127 Pisa, Italy

[60]Princeton University, Princeton, New Jersey 08544, USA

[61a]INFN Sezione di Roma, I-00185 Roma, Italy

[61b]Dipartimento di Fisica, Università di Roma La Sapienza, I-00185 Roma, Italy

[62]Universität Rostock, D-18051 Rostock, Germany

[63]Rutherford Appleton Laboratory, Chilton, Didcot, Oxon, OX11 0QX, United Kingdom

[64]CEA, Irfu, SPP, Centre de Saclay, F-91191 Gif-sur-Yvette, France

[65]SLAC National Accelerator Laboratory, Stanford, California 94309, USA

[66]University of South Carolina, Columbia, South Carolina 29208, USA

[67]Stanford University, Stanford, California 94305-4060, USA

[68]State University of New York, Albany, New York 12222, USA

[69]Tel Aviv University, School of Physics and Astronomy, Tel Aviv, 69978, Israel

[70]University of Tennessee, Knoxville, Tennessee 37996, USA

[71]University of Texas at Austin, Austin, Texas 78712, USA

[72]University of Texas at Dallas, Richardson, Texas 75083, USA

[73a]INFN Sezione di Torino, I-10125 Torino, Italy

[73b]Dipartimento di Fisica Sperimentale, Università di Torino, I-10125 Torino, Italy

[74a]INFN Sezione di Trieste, I-34127 Trieste, Italy

[74b]Dipartimento di Fisica, Università di Trieste, I-34127 Trieste, Italy

[*]Deceased.

[†]Now at Temple University, Philadelphia, Pennsylvania 19122, USA.

[‡]Also with Università di Perugia, Dipartimento di Fisica, Perugia, Italy.

[§]Also with Università di Roma La Sapienza, I-00185 Roma, Italy.

[‖]Now at University of South Alabama, Mobile, Alabama 36688, USA.

[¶]Also with Laboratoire de Physique Nucléaire et de Hautes Energies, IN2P3/CNRS, Université Pierre et Marie Curie-Paris6, Université Denis Diderot-Paris7, F-75252 Paris, France.

[**]Also with Università di Sassari, Sassari, Italy.

[75]*IFIC, Universitat de Valencia-CSIC, E-46071 Valencia, Spain*
[76]*University of Victoria, Victoria, British Columbia, Canada V8W 3P6*
[77]*Department of Physics, University of Warwick, Coventry CV4 7AL, United Kingdom*
[78]*University of Wisconsin, Madison, Wisconsin 53706, USA*

We report measurements of the branching fractions of neutral and charged B meson decays to final states containing a $K_1(1270)$ or $K_1(1400)$ meson and a charged pion. The data, collected with the *BABAR* detector at the SLAC National Accelerator Laboratory, correspond to 454×10^6 $B\bar{B}$ pairs produced in e^+e^- annihilation. We measure the branching fractions $\mathcal{B}(B^0 \rightarrow K_1(1270)^+\pi^- + K_1(1400)^+\pi^-) = 3.1^{+0.8}_{-0.7} \times 10^{-5}$ and $\mathcal{B}(B^+ \rightarrow K_1(1270)^0\pi^+ + K_1(1400)^0\pi^+) = 2.9^{+2.9}_{-1.7} \times 10^{-5}$ ($< 8.2 \times 10^{-5}$ at 90% confidence level), where the errors are statistical and systematic combined. The B^0 decay mode is observed with a significance of 7.5σ, while a significance of 3.2σ is obtained for the B^+ decay mode. Based on these results, we estimate the weak phase $\alpha = (79 \pm 7 \pm 11)°$ from the time-dependent CP asymmetries in $B^0 \rightarrow a_1(1260)^\pm \pi^\mp$ decays.

I. INTRODUCTION

B meson decays to final states containing an axial-vector meson (A) and a pseudoscalar meson (P) have been studied both theoretically and experimentally. Theoretical predictions for the branching fractions (BFs) of these decays have been calculated assuming a naïve factorization hypothesis [1,2] and QCD factorization [3]. These decay modes are expected to occur with BFs of order 10^{-6}. Branching fractions of B meson decays with an $a_1(1260)$ or $b_1(1235)$ meson plus a pion or a kaon in the final state have recently been measured [4,5].

The *BABAR* Collaboration has measured CP-violating asymmetries in $B^0 \rightarrow a_1(1260)^\pm \pi^\mp$ decays and determined an effective value α_{eff} [6] for the phase angle α of the Cabibbo-Kobayashi-Maskawa (CKM) quark-mixing matrix [7]. In the absence of penguin (loop) contributions in these decay modes, α_{eff} coincides with α.

The $\Delta S = 1$ decays we examine here are particularly sensitive to the presence of penguin amplitudes because their CKM couplings are larger than the corresponding $\Delta S = 0$ penguin amplitudes. Thus measurements of the decay rates of the $\Delta S = 1$ transitions involving the same SU(3) flavor multiplet as $a_1(1260)$ provide constraints on $\Delta \alpha = \alpha_{\text{eff}} - \alpha$ [8]. Similar SU(3)-based approaches have been proposed for the extraction of α in the $\pi^+ \pi^-$ [9], $\rho^\pm \pi^\mp$ [8], and $\rho^+ \rho^-$ channels [10,11].

The rates of $B \rightarrow K_{1A}\pi$ decays, where the K_{1A} meson is the SU(3) partner of $a_1(1260)$ and a nearly equal admixture of the $K_1(1270)$ and $K_1(1400)$ resonances [12], can be derived from the rates of $B \rightarrow K_1(1270)\pi$ and $B \rightarrow K_1(1400)\pi$ decays. For $B^0 \rightarrow K_1(1400)^+\pi^-$ [13] and $B^+ \rightarrow K_1(1400)^0\pi^+$ decays there exist experimental upper limits at the 90% confidence level (C.L.) of 1.1×10^{-3} and 2.6×10^{-3}, respectively [14]. In the following, K_1 will be used to indicate both $K_1(1270)$ and $K_1(1400)$ mesons.

The production of K_1 mesons in B decays has been previously observed in the $B \rightarrow J/\psi K_1$, $B \rightarrow K_1 \gamma$, and $B \rightarrow K_1 \phi$ decay channels [15]. Here we present measure-

ments of the $B^0 \rightarrow K_1^+ \pi^-$ and $B^+ \rightarrow K_1^0 \pi^+$ branching fractions and estimate the weak phase α from the measurement of the time-dependent CP asymmetries in $B^0 \rightarrow a_1(1260)^\pm \pi^\mp$ decays and the branching fractions of SU(3) related modes.

This paper is organized as follows. In Sec. II we describe the data set and the detector. In Sec. III we introduce the K-matrix formalism used for the parametrization of the K_1 resonances. Section IV is devoted to a discussion of the reconstruction and selection of the B candidates. In Sec. V we describe the maximum-likelihood fit for the signal branching fractions and the likelihood scan over the parameters that characterize the production of the K_1 system. In Sec. VI we discuss the systematic uncertainties. In Sec. VII we present the experimental results. Finally, in Sec. VIII, we use the experimental results to extract bounds on $|\Delta \alpha|$.

II. THE *BABAR* DETECTOR AND DATA SET

The results presented in this paper are based on data collected with the *BABAR* detector at the PEP-II asymmetric-energy e^+e^- storage ring, operating at the SLAC National Accelerator Laboratory. At PEP-II, 9.0 GeV electrons collide with 3.1 GeV positrons to yield a center-of-mass (CM) energy of $\sqrt{s} = 10.58$ GeV, which corresponds to the mass of the $\Upsilon(4S)$ resonance. The asymmetric energies result in a boost from the laboratory to the CM frame of $\beta\gamma \approx 0.56$. We analyze the final *BABAR* data set collected at the $\Upsilon(4S)$ resonance, corresponding to an integrated luminosity of 413 fb^{-1} and $N_{B\bar{B}} = (454.3 \pm 5.0) \times 10^6$ produced $B\bar{B}$ pairs.

A detailed description of the *BABAR* detector can be found elsewhere [16]. Surrounding the interaction point is a five-layer double-sided silicon vertex tracker (SVT) that provides precision measurements near the collision point of charged particle tracks in the planes transverse to and along the beam direction. A 40-layer drift chamber surrounds the SVT. Both of these tracking devices operate in

the 1.5 T magnetic field of a superconducting solenoid to provide measurements of the momenta of charged particles. Charged hadron identification is achieved through measurements of particle energy loss in the tracking system and the Cherenkov angle obtained from a detector of internally reflected Cherenkov light. A CsI(Tl) electromagnetic calorimeter provides photon detection and electron identification. Finally, the instrumented flux return (IFR) of the magnet allows discrimination of muons from pions and detection of K_L^0 mesons. For the first 214 fb^{-1} of data, the IFR was composed of a resistive plate chamber system. For the most recent 199 fb^{-1} of data, a portion of the resistive plate chamber system has been replaced by limited streamer tubes [17].

We use a GEANT4-based Monte Carlo (MC) simulation to model the response of the detector [18], taking into account the varying accelerator and detector conditions. We generate large samples of signal and background for the modes considered in the analysis.

III. SIGNAL MODEL

In this analysis the signal is characterized by two nearby resonances, $K_1(1270)$ and $K_1(1400)$, which have the same quantum numbers, $I(J^P) = 1/2(1^+)$, and decay predominantly to the same $K\pi\pi$ final state. The world's largest sample of $K_1(1270)$ and $K_1(1400)$ events was collected by the ACCMOR Collaboration with the WA3 experiment [19]. The WA3 fixed target experiment accumulated data from the reaction $K^- p \rightarrow K^- \pi^+ \pi^- p$ with an incident kaon energy of 63 GeV. These data were analyzed using a two-resonance, six-channel K-matrix model [20] to describe the resonant $K\pi\pi$ system. We base our parametrization of the K_1 resonances produced in B decays on a model derived from the K-matrix description of the scattering amplitudes in Ref. [19]. In Sec. III A we briefly outline the K-matrix formalism, which is then applied in Sec. III B to fit the ACCMOR data in order to determine the parameters describing the diffractive production of K_1 mesons and their decay. In Sec. III C we explain how we use the extracted values of the decay parameters and describe our model for K_1 production in $B \rightarrow (K\pi\pi)\pi$ decays.

A. K-matrix formalism

Following the analysis of the ACCMOR Collaboration, the $K\pi\pi$ system is described by a K-matrix model comprising six channels, $1 = (K^*(892)\pi)_S$, $2 = \rho K$, $3 = K_0^*(1430)\pi$, $4 = f_0(1370)K$, $5 = (K^*(892)\pi)_D$, $6 = \omega K$. We identify each channel by the intermediate resonance and bachelor particle, where the bachelor particle is the π or K produced directly from the K_1 decay. For the $K^*(892)\pi$ channels the subscript refers to the angular momentum.

We parametrize the production amplitude for each channel in the reaction $K^- p \rightarrow (K^- \pi^+ \pi^-)p$ as

$$F_i = e^{i\delta_i} \sum_j (\mathbf{1} - i\mathbf{K}\boldsymbol{\rho})_{ij}^{-1} P_j, \tag{1}$$

where the index i (and similarly j) represents the ith channel. The elements of the diagonal phase-space matrix $\boldsymbol{\rho}(M)$ for the decay chain

$$K_1 \rightarrow V_3 + h_4, \qquad V_3 \rightarrow h_5 + h_6, \qquad h = \pi, K \tag{2}$$

are approximated with the form

$$\rho_{ij}(M) = \frac{2\delta_{ij}}{M}\sqrt{\frac{2m^* m_4}{m^* + m_4}(M - m^* - m_4 + i\Delta)}, \tag{3}$$

where M is the $K\pi\pi$ invariant mass, m_4 is the mass of the bachelor particle h_4, and m^* (Δ) is the pole mass (half width) of the intermediate resonance state V_3 [21]. In Eq. (1), the δ_i parameters are offset phases with respect to the $(K^*(892)\pi)_S$ channel ($\delta_1 \equiv 0$). The 6×6 K-matrix **K** has the following form:

$$K_{ij} = \frac{f_{ai}f_{aj}}{M_a - M} + \frac{f_{bi}f_{bj}}{M_b - M}, \tag{4}$$

where the labels a and b refer to $K_1(1400)$ and $K_1(1270)$, respectively. The decay constants f_{ai}, f_{bi} and the K-matrix poles M_a and M_b are real. The production vector **P** consists of a background term **D** [22] and a direct production term **R**, according to the following relation among vector elements:

$$P_i = R_i + \sum_j (1 + i\tau K_{ij})D_j, \tag{5}$$

where τ is a constant.

The background amplitudes are parametrized by

$$D_i = D_{i0}\frac{e^{i\phi_i}}{M^2 - M_K^2} \tag{6}$$

for all channels but $(K^*(892)\pi)_D$ and ωK. For the $(K^*(892)\pi)_D$ channel we set $D_5 = 0$ as in the ACCMOR analysis [19]. The parameters for the ωK channel are not fitted, as described later in this section, and we set $D_6 = 0$. The results are not sensitive to this choice for the value of D_6.

R is given by

$$R_i = \frac{f_{pa}f_{ai}}{M_a - M} + \frac{f_{pb}f_{bi}}{M_b - M}, \tag{7}$$

where f_{pa} and f_{pb} represent the amplitude for producing the states $K_1(1400)$ and $K_1(1270)$, respectively, and are complex numbers. We assume f_{pa} to be real.

P-wave ($\ell = 1$) and D-wave ($\ell = 2$) centrifugal barrier factors are included in the K_1 decay couplings f_{ai} and f_{bi} and background amplitudes D_{i0}, and are given by

$$B_i(M) = \left[\frac{q_i(M)^2 R^2}{1 + q_i(M)^2 R^2}\right]^{\ell/2}, \tag{8}$$

where q_i is the breakup momentum in channel i. Typical values for the interaction radius squared R^2 are in the range

$5 < R^2 < 100$ GeV^{-2} [23] and the value $R^2 = 25$ GeV^{-2} is used.

The physical resonances $K_1(1270)$ and $K_1(1400)$ are mixtures of the two SU(3) octet states K_{1A} and K_{1B}:

$$|K_1(1400)\rangle = |K_{1A}\rangle \cos\theta + |K_{1B}\rangle \sin\theta, \qquad (9)$$

$$|K_1(1270)\rangle = -|K_{1A}\rangle \sin\theta + |K_{1B}\rangle \cos\theta. \qquad (10)$$

Assuming that SU(3) violation manifests itself only in the mixing, we impose the following relations [19]:

$$f_{a1} = \frac{1}{2}\gamma_+ \cos\theta + \sqrt{\frac{9}{20}}\gamma_- \sin\theta, \qquad (11)$$

$$f_{b1} = -\frac{1}{2}\gamma_+ \sin\theta + \sqrt{\frac{9}{20}}\gamma_- \cos\theta, \qquad (12)$$

$$f_{a2} = \frac{1}{2}\gamma_+ \cos\theta - \sqrt{\frac{9}{20}}\gamma_- \sin\theta, \qquad (13)$$

$$f_{b2} = -\frac{1}{2}\gamma_+ \sin\theta - \sqrt{\frac{9}{20}}\gamma_- \cos\theta, \qquad (14)$$

where γ_+ and γ_- are the couplings of the SU(3) octet states to the $(K^*(892)\pi)_S$ and ρK channels: $\langle (K^*(892)\pi)_S | K_{1A}\rangle = \frac{1}{2}\gamma_+ = \langle\rho K | K_{1A}\rangle$ and $\langle\rho K | K_{1B}\rangle = -\sqrt{\frac{9}{20}}\gamma_- = -\langle (K^*(892)\pi)_S | K_{1B}\rangle$. The couplings for the ωK channel are fixed to $1/\sqrt{3}$ of the ρK couplings, as follows from the quark model [19].

B. Fit to WA3 data

Only some of the K-matrix parameters extracted in the ACCMOR analysis have been reported in the literature [19]. In particular, the results for most of the decay couplings f_{ai} and f_{bi} are not available. The ACCMOR Collaboration performed a partial-wave analysis of the WA3 data. The original WA3 paper [19] provides the results of the partial-wave analysis of the $K\pi\pi$ system in the form of plots for the intensity in the $(K^*(892)\pi)_S$, ρK, $K_0^*(1430)\pi$, $f_0(1370)K$, and $(K^*(892)\pi)_D$ channels, together with the phases of the corresponding amplitudes, measured relative to the $(K^*(892)\pi)_S$ amplitude. The ωK data were not analyzed. In order to obtain an estimate of the parameters that enter the K-matrix model, we perform a χ^2 fit of this model to the $0 \le |t'| \le 0.05$ GeV^2 WA3 data for the intensity of the $m = 0$ $K\pi\pi$ channels and the relative phases. Here $|t'|$ is the four momentum transfer squared with respect to the recoiling proton in the reaction $K^- p \rightarrow K^- \pi^+ \pi^- p$, and m denotes the magnetic substate of the $K\pi\pi$ system. Since the results of the analysis performed by the ACCMOR Collaboration are not sensitive to the choice of the value for the constant τ in Eq. (5), we set $\tau = 0$. We seek solutions corresponding to positive values of the $\gamma_\pm$ parameters, as found in the ACCMOR

analysis [19]. The data sample consists of 215 bins. The results of this fit are displayed in Fig. 1 and show a good qualitative agreement with the results obtained by the ACCMOR Collaboration [19]. We obtain $\chi^2 = 855$, with 26 free parameters, while the ACCMOR Collaboration obtained $\chi^2 = 529$. We interpret this difference as due to slight inaccuracies in extracting the errors on the data points from the WA3 paper [19]. These discrepancies do not appreciably affect the extracted central values and errors of the parameters of the model, summarized in Table I, and are therefore innocuous for the purposes of the present work. Although neither fit is formally a good one, the model succeeds in reproducing the relevant features of the data.

C. Model for K_1 production in B decays

We apply the above formalism to the parametrization of the signal component for the production of K_1 resonances
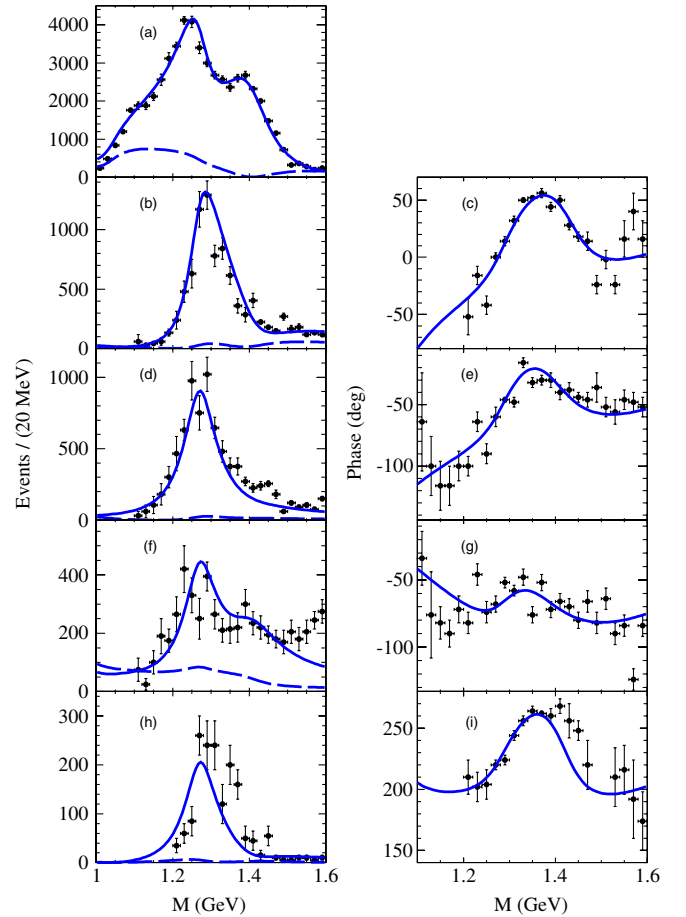
FIG. 1 (color online). Results of the fit to the $0 \le |t'| \le 0.05$ GeV^2 WA3 data. Intensity (left) and phase relative to the $(K^*(892)\pi)_S$ amplitude (right) for the (a) $(K^*(892)\pi)_S$, (b, c) ρK, (d, e) $K_0^*(1430)\pi$, (f, g) $f_0(1370)K$, and (h, i) $(K^*(892)\pi)_D$ channels. The points represent the data, the solid lines the total fit function, and the dashed lines the contribution from the background.

TABLE I. Parameters for the K-matrix model used in the analysis of B decays.

Parameter	Fitted value
M_a	1.40 ± 0.02
M_b	1.16 ± 0.02
θ	$72° \pm 3°$
γ_+	0.75 ± 0.03
γ_-	0.44 ± 0.03
f_{a3}	0.02 ± 0.03
f_{b3}	0.32 ± 0.01
f_{a4}	-0.08 ± 0.02
f_{b4}	0.16 ± 0.01
f_{a5}	0.06 ± 0.01
f_{b5}	0.21 ± 0.04
δ_2	$-31° \pm 1°$
δ_3	$82° \pm 2°$
δ_4	$78° \pm 4°$
δ_5	$20° \pm 9°$

in B decays. The propagation of the uncertainties in the K-matrix description of the ACCMOR data to the model for K_1 production in B decays is a source of systematic uncertainty and is taken into account as described in Sec. VI.

In order to parametrize the signal component for the analysis of B decays, we set the background amplitudes **D**, whose contribution should be small in the nondiffractive case, to 0. The backgrounds arising from resonant and nonresonant B decays to the $(K\pi\pi)\pi$ final state are taken into account by separate components in the fit, as described in Sec. V. The parameters of **K** and the offset phases δ_i are assumed to be independent from the production process and are fixed to the values extracted from the fit to WA3 data (Table I). Finally, we express the production couplings f_{pa} and f_{pb} in terms of two real production parameters $\zeta = (\vartheta, \phi)$: $f_{pa} \equiv \cos\vartheta$, $f_{pb} \equiv \sin\vartheta e^{i\phi}$, where $\vartheta \in [0, \pi/2]$, $\phi \in [0, 2\pi]$. In this parametrization, $\tan\vartheta$ represents the magnitude of the production constant for the $K_1(1270)$ resonance relative to that for the $K_1(1400)$ resonance, while ϕ is the relative phase.

The dependence of the selection efficiencies and of the distribution of the discriminating variables (described in Sec. V) on the production parameters ζ are derived from Monte Carlo studies. For given values of ζ, signal MC samples for B decays to the $(K\pi\pi)\pi$ final states are generated by weighting the $(K\pi\pi)\pi$ population according to the amplitude $\sum_{i \neq \omega K} \langle K\pi\pi|i\rangle F_i$, where the term $\langle K\pi\pi|i\rangle$ consists of a factor describing the angular distribution of the $K\pi\pi$ system resulting from K_1 decay, an amplitude for the resonant $\pi\pi$ and $K\pi$ systems, and isospin factors, and is calculated using the formalism described in Refs. [19,24]. The ωK channel is excluded from the sum, since the $\omega \rightarrow \pi^+\pi^-$ branching fraction is only $(1.53^{+0.11}_{-0.13})\%$, compared to the branching fraction $(89.2 \pm 0.7)\%$ of the dominant decay $\omega \rightarrow \pi^+\pi^-\pi^0$ [12].

Most of the $K_1 \rightarrow \omega K$ decays therefore result in a different final state than the simulated one. We account for the $K_1 \rightarrow \omega K$ transitions with a correction to the overall efficiency. In Fig. 2 we show the reference frame chosen to evaluate the distributions of the products of $B \rightarrow K_1\pi$ decays, where K_1 decays proceed through the intermediate resonances $X_s = \{K^*(892), K_0^*(1430)\}$ or $X_d = \{\rho, f_0(1370), \omega\}$. Final state particles are labeled with a subscript $\{k, l, m, n\}$, according to the following scheme: $B^0 \rightarrow K_1^+ \pi_k^-$, $K_1^+ \rightarrow X_s^0\pi_l^+$ $X_s^0 \rightarrow K_m^+\pi_n^-$ or $B^0 \rightarrow K_1^+\pi_k^-$, $K_1^+ \rightarrow X_d^0K_l^+$, $X_d^0 \rightarrow \pi_m^+\pi_n^-$ for neutral B meson decays, and $B^+ \rightarrow K_1^0\pi_k^+$, $K_1^0 \rightarrow X_s^+\pi_l^-$, $X_s^+ \rightarrow K_m^0\pi_n^+$ or $B^+ \rightarrow K_1^0\pi_k^+$, $K_1^0 \rightarrow X_d^0K_l^0$, $X_d^0 \rightarrow \pi_m^+\pi_n^-$ for charged B meson decays. The angular distribution for the K_1 system produced in B decays can be expressed in terms of three independent angles (Θ, β, Φ). In the K_1 rest frame, we define the Y axis as the normal to the decay plane of the K_1, and orient the Z axis along the momentum of l [Fig. 2(a)]. Θ and Φ are then the polar and azimuthal angles of the momentum of k, respectively, in the K_1 rest frame [Fig. 2(b)]. We define β as the polar angle of the flight direction of m relative to the direction of the momentum of l [Fig. 2(c)]. The resulting angular parts of the transition amplitudes for S-, P-, and D-wave decays of the K_1 axial-vector ($J^P = 1^+$) mesons with scalar ($J^P = 0^+$) and vector ($J^P = 1^-$) intermediate resonances $X_{s,d}$ are given by

$$A_S = \sqrt{\frac{3}{8\pi}}(\cos\Theta \cos\beta + \sin\Theta \sin\beta \cos\Phi) \quad (15)$$

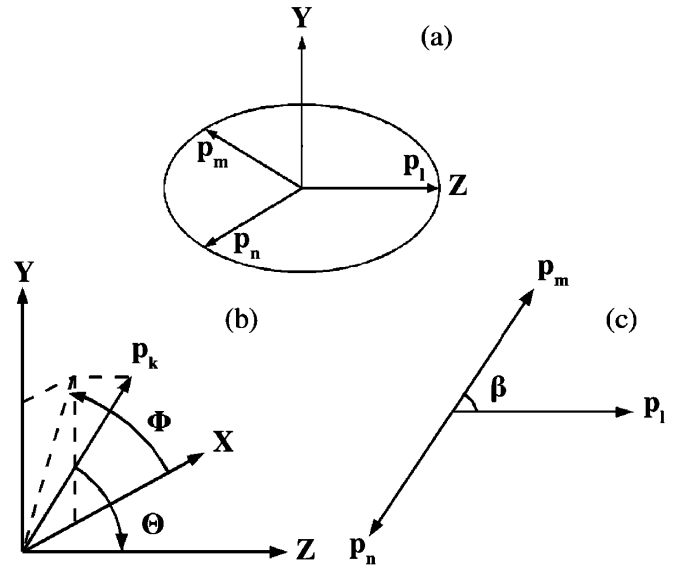$$A_P = \sqrt{\frac{3}{8\pi}}\cos\Theta \quad (16)$$

FIG. 2. Definition of (a) the coordinate axes in the K_1 rest frame, (b) the angles Θ and Φ in the K_1 rest frame, and (c) the angle β in the rest frame of the $X_{s,d}$ intermediate resonance.

$$A_D = \sqrt{\frac{3}{16\pi}}(-2\cos\Theta\cos\beta + \sin\Theta\sin\beta\cos\Phi). \quad (17)$$

For the $\pi\pi$ and $K\pi$ resonances, the following ℓ-wave Breit-Wigner parameterization is used [24]:

$$BW(m) = (\pi)^{-1/2}\frac{[m_0\Gamma(m)]^{1/2}}{(m_0^2 - m^2) - im_0\Gamma(m)} \quad (18)$$

with

$$\Gamma(m) = \Gamma(m_0)\frac{m_0}{m}\left[\frac{q(m)}{q(m_0)}\right]^{2\ell+1}\left[\frac{1 + R^2q^2(m_0)}{1 + R^2q^2(m)}\right]^\ell, \quad (19)$$

where m_0 is the nominal mass of the resonance, $\Gamma(m)$ is the mass-dependent width, $\Gamma(m_0)$ is the nominal width of the resonance, q is the breakup momentum of the resonance into the two-particle final state, and $R^2 = 25$ GeV^{-2}. The $K_0^*(1430)$ and $f_0(1370)$ amplitudes are also parametrized as Breit-Wigner functions. For the $K_0^*(1430)$ we assume a mass of 1.250 GeV and a width of 0.600 GeV [19], while for the $f_0(1370)$ we use a mass of 1.256 GeV and a width of 0.400 GeV [25]. This parametrization is varied in Sec. VI and a systematic uncertainty evaluated.

IV. EVENT RECONSTRUCTION AND SELECTION

The $B^0 \to K_1^+\pi^-$ candidates are reconstructed in the $K_1^+ \to K^+\pi^+\pi^-$ decay mode by means of a vertex fit of all combinations of four charged tracks having a zero net charge. Similarly we reconstruct $B^+ \to K_1^0\pi^+$ candidates, with $K_1^0 \to K_S^0\pi^+\pi^-$, by combining K_S^0 candidates with three charged tracks. We require the reconstructed mass $m_{K\pi\pi}$ to lie in the range [1.1, 1.8] GeV. Charged particles are identified as either pions or kaons, and must not be consistent with the electron, muon or proton hypotheses. The K_S^0 candidates are reconstructed from pairs of oppositely charged pions with an invariant mass in the range [486, 510] MeV, whose decay vertex is required to be displaced from the K_1 vertex by at least 3 standard deviations.

The reconstructed B candidates are characterized by two almost uncorrelated variables, the energy-substituted mass

$$m_{ES} \equiv \sqrt{\left(\frac{1}{2}s + \mathbf{p}_0\cdot\mathbf{p}_B\right)^2/E_0^2 - \mathbf{p}_B^2} \quad (20)$$

and the energy difference

$$\Delta E \equiv E_B^* - \frac{1}{2}\sqrt{s}, \quad (21)$$

where $(E_0, \mathbf{p}_0)$ and $(E_B, \mathbf{p}_B)$ are the laboratory four-momenta of the $\Upsilon(4S)$ and the B candidate, respectively, and the asterisk denotes the CM frame. We require $5.25 < m_{ES} < 5.29$ GeV and $|\Delta E| < 0.15$ GeV. For correctly reconstructed B candidates, the distribution of m_{ES} peaks at the B-meson mass and ΔE at zero.

Background events arise primarily from random combinations of particles in continuum $e^+e^- \to q\bar{q}$ events ($q = u, d, s, c$). We also consider cross feed from other B meson decay modes than those in the signal.

To separate continuum from $B\bar{B}$ events we use variables that characterize the event shape. We define the angle θ_T between the thrust axis [26] of the B candidate in the $\Upsilon(4S)$ frame and that of the charged tracks and neutral calorimeter clusters in the rest of the event. The distribution of $|\cos\theta_T|$ is sharply peaked near 1 for $q\bar{q}$ jet pairs and nearly uniform for B-meson decays. We require $|\cos\theta_T| < 0.8$. We construct a Fisher discriminant $\mathcal{F}$ from a linear combination of four topological variables: the monomials $L_0 = \sum_i p_i^*$ and $L_2 = \sum_i p_i^*|\cos\theta_i^*|^2$, $|\cos\theta_C^*|$ and $|\cos\theta_B^*|$ [27]. Here, p_i^* and θ_i^* are the CM momentum and the angle of the remaining tracks and clusters in the event with respect to the B candidate thrust axis. θ_C^* and θ_B^* are the CM polar angles of the B-candidate thrust axis and B-momentum vector, respectively, relative to the beam axis. In order to improve the accuracy in the determination of the event shape variables, we require a minimum of 5 tracks in each event.

Background from B decays to final states containing charm or charmonium mesons is suppressed by means of vetos. A signal candidate is rejected if it shares at least one track with a B candidate reconstructed in the $B^0 \to D^-\pi^+$, $B^0 \to D^{*-}\pi^+$, $B^+ \to \bar{D}^0\pi^+$, or $B^+ \to \bar{D}^{*0}\pi^+$ decay modes, where the D meson in the final states decays hadronically. A signal candidate is also discarded if any $\pi^+\pi^-$ combination consisting of the primary pion from the B decay together with an oppositely charged pion from the K_1 decay has an invariant mass consistent with the $c\bar{c}$ mesons $\chi_{c0}(1P)$ or $\chi_{c1}(1P)$ decaying to a pair of oppositely charged pions, or J/ψ and $\psi(2S)$ decaying to muons where the muons are misidentified as pions.

We define $\mathcal{H}$ as the cosine of the angle between the direction of the primary pion from the B decay and the normal to the plane defined by the K_1 daughter momenta in the K_1 rest frame. We require $|\mathcal{H}| < 0.95$ to reduce background from $B \to V\pi$ decay modes, where V is a vector meson decaying to $K\pi\pi$, such as $K^*(1410)$ or $K^*(1680)$.

The average number of candidates in events containing at least one candidate is 1.2. In events with multiple candidates, we select the candidate with the highest χ^2 probability of the B vertex fit.

We classify the events according to the invariant masses of the $\pi^+\pi^-$ and $K^+\pi^-(K_S^0\pi^+)$ systems in the $K_1^+(K_1^0)$ decay for $B^0(B^+)$ candidates: events that satisfy the requirement $0.846 < m_{K\pi} < 0.946$ GeV belong to class 1 ("K^* band"); events not included in class 1 for which $0.500 < m_{\pi\pi} < 0.800$ GeV belong to class 2 ("ρ band"); all other events are rejected. The fractions of selected signal events in class 1 and class 2 range from 33% to 73% and from 16% to 49%, respectively, depending on the production parameters ζ. About 11% to 19% of

the signal events are rejected at this stage. For combinatorial background, the fractions of selected events in class 1 and class 2 are 22% and 39%, respectively, while 39% of the events are rejected.

The signal reconstruction and selection efficiencies depend on the production parameters ζ. For B^0 modes these efficiencies range from 5 to 12% and from 3 to 8% for events in class 1 and class 2, respectively. For B^+ modes the corresponding values are 4–9% and 2–7%.

V. MAXIMUM-LIKELIHOOD FIT

We use an unbinned, extended maximum-likelihood (ML) fit to extract the event yields $n_{s,r}$ and the parameters of the probability density function (PDF) $\mathcal{P}_{s,r}$. The subscript $r = \{1, 2\}$ corresponds to one of the resonance band classes defined in Sec. IV. The index s represents the event categories used in our fit model. For the analysis of B^0 modes, these are

   (1) signal,
   (2) combinatorial background,
   (3) $B^0 \rightarrow K^*(1410)^+ \pi^-$,
   (4) $B^0 \rightarrow K^*(892)^0 \pi^+ \pi^- + \rho^0 K^+ \pi^-$,
   (5) $B^0 \rightarrow a_1(1260)^\pm \pi^\mp$, and
   (6) $B^0 \rightarrow D^-_{K\pi\pi} \pi^+$.

For B^+ modes, these are

   (1) signal,
   (2) combinatorial background,
   (3) $B^+ \rightarrow K^*(1410)^0 \pi^+$,
   (4) $B^+ \rightarrow K^*(892)^+ \pi^+ \pi^- + \rho^0 K^0_S \pi^+$, and
   (5) $B^+ \rightarrow K^*(892)^+ \rho^0$.

The likelihood $\mathcal{L}_{e,r}$ for a candidate e to belong to class r is defined as

$$\mathcal{L}_{e,r} = \sum_s n_{s,r} \mathcal{P}_{s,r}(\mathbf{x}_e; \zeta, \xi), \qquad (22)$$

where the PDFs are formed using the set of observables $\mathbf{x}_e = \{\Delta E, m_{\mathrm{ES}}, \mathcal{F}, m_{K\pi\pi}, |\mathcal{H}|\}$ and the dependence on the production parameters ζ is relevant only for the signal PDF. ξ represents all other PDF parameters.

In the definition of $\mathcal{L}_{e,r}$ the yields of the signal category for the two classes are expressed as a function of the signal branching fraction $\mathcal{B}$ as $n_{1,1} = \mathcal{B} \times N_{B\bar{B}} \times \epsilon_1(\zeta)$ and $n_{1,2} = \mathcal{B} \times N_{B\bar{B}} \times \epsilon_2(\zeta)$, where the total selection efficiency $\epsilon_r(\zeta)$ includes the daughter branching fractions and the reconstruction efficiency obtained from MC samples as a function of the production parameters.

For the B^0 modes we perform a negative log-likelihood scan with respect to ϑ and ϕ. Although the events in class $r = 2$ are characterized by a smaller signal-to-background ratio with respect to the events in class $r = 1$, MC studies show that including these events in the fit for the B^0 modes helps to resolve ambiguities in the determination of ϕ in cases where a signal is observed. At each point of the scan, a simultaneous fit to the event classes $r = 1, 2$ is performed.

For the B^+ modes, simulations show that, due to a less favorable signal-to-background ratio and increased background from B decays, we are not sensitive to ϕ over a wide range of possible values of the signal BF. We therefore assume $\phi = \pi$ and restrict the scan to ϑ. At each point of the scan, we perform a fit to the events in class $r = 1$ only. The choice $\phi = \pi$ minimizes the variations in the fit results associated with differences between the $m_{K\pi\pi}$ PDFs for different values of ϕ. This source of systematic uncertainty is accounted for as described in Sec. VI. The variations in the efficiency ϵ_1 as a function of ϕ for a given ϑ can be as large as 30%, and are taken into account in deriving the branching fraction results as discussed in Sec. VII.

The fitted samples consist of 23167 events (B^0 modes, class 1), 38005 events (B^0 modes, class 2), and 9630 events (B^+ modes, class 1).

The signal branching fractions are free parameters in the fit. The yields for event categories $s = 5, 6$ (B^0 modes) and $s = 5$ (B^+ modes) are fixed to the values estimated from MC simulated data and based on their previously measured branching fractions [12,28]. The yields for the other background components are determined from the fit. The PDF parameters for combinatorial background are left free to vary in the fit, while those for the other event categories are fixed to the values extracted from MC samples.

The signal and background PDFs are constructed as products of PDFs describing the distribution of each observable. The assumption of negligible correlations in the selected data samples among the discriminating variables has been tested with MC samples. The PDFs for ΔE and m_{ES} of the categories 1, 3, 4, and 5 are each parametrized as a sum of a Gaussian function to describe the core of each distribution, plus an empirical function determined from MC simulated data to account for the tails of each distribution. For the combinatorial background we use a first-degree Chebyshev polynomial for ΔE and an empirical phase-space function [29] for m_{ES}:

$$f(x) \propto x\sqrt{1 - x^2}\, \exp[-\xi_1(1 - x^2)], \qquad (23)$$

where $x \equiv 2m_{\mathrm{ES}}/\sqrt{s}$ and ξ_1 is a parameter that is determined from the fit. The combinatorial background PDF is found to describe well both the dominant quark-antiquark background and the background from random combinations of B tracks.

For all categories the $\mathcal{F}$ distribution is well described by a Gaussian function with different widths to the left and right of the mean. A second Gaussian function with a larger width accounts for a small tail in the distribution and prevents the background probability from becoming too small in the signal $\mathcal{F}$ region.

The $m_{K\pi\pi}$ distribution for the signal depends on ζ. To each point of the ζ scan, we therefore associate a different nonparametric template, modeled upon signal MC samples reweighted according to the corresponding values of the

production parameters ϑ and ϕ. Production of $K^*(1410)$ and $a_1(1260)$ resonances occurs in B background and is taken into account in the $m_{K\pi\pi}$ and $|\mathcal{H}|$ PDFs. For all components, the PDFs for $|\mathcal{H}|$ are parametrized with polynomials.

We use large control samples to verify the m_{ES}, ΔE, and $\mathcal{F}$ PDF shapes, which are initially determined from MC samples. We use the $B^0 \to D^- \pi^+$ decay with $D^- \to K^+ \pi^- \pi^-$, and the $B^+ \to \bar{D}^0 \pi^-$ decay with $D^0 \to K_S^0 \pi^+ \pi^-$, which have similar topology to the signal B^0 and B^+ modes, respectively. We select these samples by applying loose requirements on m_{ES} and ΔE, and requiring for the D candidate mass $1848 < m_{D^-} < 1890$ MeV and $1843 < m_{D^0} < 1885$ MeV. The selection requirements on the B and D daughters are very similar to those of our signal modes. These selection criteria are applied both to the data and to the MC events. There is good agreement between data and MC samples: the deviations in the means of the distributions are about 0.5 MeV for m_{ES}, 3 MeV for ΔE, and negligible for $\mathcal{F}$.

VI. SYSTEMATIC UNCERTAINTIES

The main sources of systematic uncertainties are summarized in Table II. For the branching fractions, the errors that affect the result only through efficiencies are called "multiplicative" and given in percentage. All other errors are labeled "additive" and expressed in units of 10^{-6}.

TABLE II. Estimates of systematic errors, evaluated at the absolute minimum of each $-\ln\mathcal{L}$ scan. For the branching fraction, the errors labeled (A), for additive, are given in units of 10^{-6}, while those labeled (M), for multiplicative, are given in percentage.

| Quantity | $B^0 \to K_1^+ \pi^-$ | | | $B^+ \to K_1^0 \pi^+$ | |
	$\mathcal{B}$	ϑ	ϕ	$\mathcal{B}$	ϑ
PDF parameters (A)	0.8	0.01	0.15	1.4	0.07
MC/data correction (A)	0.8	0.00	0.01	1.0	0.02
ML fit bias (A)	0.6	0.03	0.02	2.0	0.08
Fixed phase (A)	$\cdots$	$\cdots$	$\cdots$	0.6	0.06
Scan (A)	0.9	0.04	0.16	0.0	0.04
K_1 K-matrix parameters (A)	2.2	0.01	0.36	0.5	0.05
K_1 offset phases (A)	0.2	0.01	0.02	0.0	0.00
K_1 intermediate resonances (A)	0.5	0.00	0.06	0.2	0.02
K^*/ρ bands (A)	0.2	0.05	0.00	1.2	0.05
Peaking $B\bar{B}$ bkg (A)	0.8	0.01	0.13	1.0	0.01
Fixed background yields (A)	0.0	0.00	0.00	0.4	0.02
Interference (A)	6.0	0.25	0.52	10.6	0.43
MC statistics (M)	1.0	$\cdots$	$\cdots$	1.0	$\cdots$
Particle identification (M)	2.9	$\cdots$	$\cdots$	3.1	$\cdots$
Track finding (M)	1.0	$\cdots$	$\cdots$	0.8	$\cdots$
K_S^0 reconstruction (M)	$\cdots$	$\cdots$	$\cdots$	1.6	$\cdots$
$\cos\theta_T$ (M)	1.0	$\cdots$	$\cdots$	1.0	$\cdots$
Track multiplicity (M)	1.0	$\cdots$	$\cdots$	1.0	$\cdots$
Number $B\bar{B}$ pairs (M)	1.1	$\cdots$	$\cdots$	1.1	$\cdots$

We repeat the fit by varying the PDF parameters ξ, within their uncertainties, that are not left floating in the fit. The signal PDF model excludes fake combinations originating from misreconstructed signal events. Potential biases due to the presence of fake combinations, or other imperfections in the signal PDF model, are estimated with MC simulated data. We also account for possible bias introduced by the finite resolution of the (ϑ, ϕ) likelihood scan. A systematic error is evaluated by varying the $K_1(1270)$ and $K_1(1400)$ mass poles and K-matrix parameters in the signal model, the parametrization of the intermediate resonances in K_1 decay, and the offset phases δ_i. We test the stability of the fit results against variations in the selection of the "K^*" and "ρ bands," and evaluate a corresponding systematic error. An additional systematic uncertainty originates from potential peaking $B\bar{B}$ background, including $B \to K_2^*(1430)\pi$ and $B \to K^*(1680)\pi$, and is evaluated by introducing the corresponding components in the definition of the likelihood and repeating the fit with their yields fixed to values estimated from the available experimental information [12]. We vary the yields of the $B^0 \to a_1(1260)^\pm \pi^\mp$ and $B^0 \to D^-_{K^+\pi^-\pi^-}\pi^+$ (for the B^0 modes) and $B^+ \to K^{*+}\rho^0$ (for the B^+ modes) event categories by their uncertainties and take the resulting change in results as a systematic error. For B^+ modes, we introduce an additional systematic uncertainty to account for the variations of the ϕ parameter. The above systematic uncertainties do not scale with the event yield and are included in the calculation of the significance of the result.

We estimate the systematic uncertainty due to the interference between the $B \to K_1\pi$ and the $B \to K^*\pi\pi + \rho K\pi$ decays using simulated samples in which the decay amplitudes are generated according to the results of the likelihood scans. The overall phases and relative contribution for the $K^*\pi\pi$ and $\rho K\pi$ interfering states are assumed to be constant across phase space and varied between zero and a maximum value using uniform prior distributions. We calculate the systematic uncertainty from the RMS variation of the average signal branching fraction and parameters. This uncertainty is assumed to scale as the square root of the signal branching fraction and does not affect the significance. The systematic uncertainties in efficiencies include those associated with track finding, particle identification and, for the B^+ modes, K_S^0 reconstruction. Other systematic effects arise from event selection criteria, such as track multiplicity and thrust angle, and the number of B mesons.

VII. FIT RESULTS

Figures 3 and 4 show the distributions of ΔE, m_{ES} and $m_{K\pi\pi}$ for the signal and combinatorial background events, respectively, obtained by the event-weighting technique $_s\mathcal{P}$lot [30]. For each event, signal and background weights are derived according to the results of the fit to all variables and the probability distributions in the restricted set of
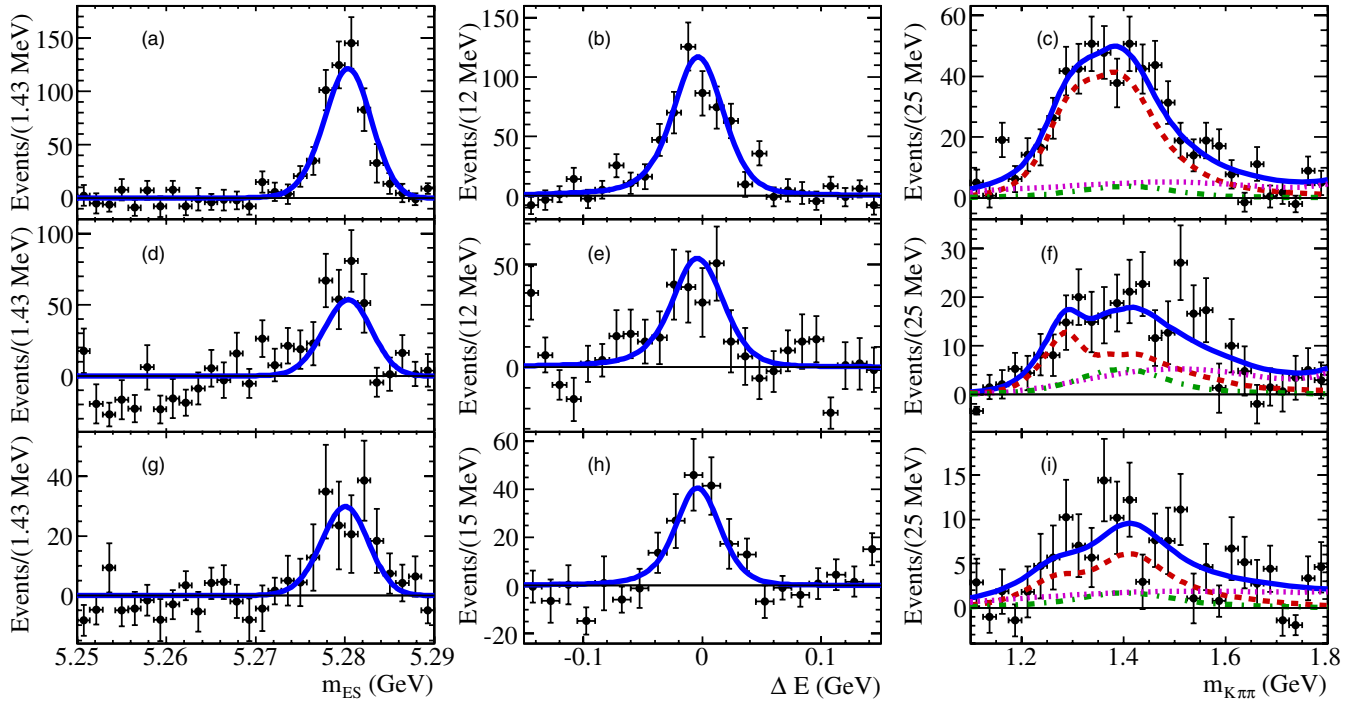
FIG. 3 (color online).   sPlot projections of signal onto m_{ES} (left), ΔE (center), and $m_{K\pi\pi}$ (right) for B^0 class 1 (top), B^0 class 2 (middle), and B^+ class 1 (bottom) events: the points show the sums of the signal weights obtained from on-resonance data. For m_{ES} and ΔE the solid line is the signal fit function. For $m_{K\pi\pi}$ the solid line is the sum of the fit functions of the decay modes $K_1(1270)\pi + K_1(1400)\pi$ (dashed), $K^*(1410)\pi$ (dash-dotted), and $K^*(892)\pi\pi$ (dotted), and the points are obtained without using information about resonances in the fit, i.e., we use only the m_{ES}, ΔE, and $\mathcal{F}$ variables.
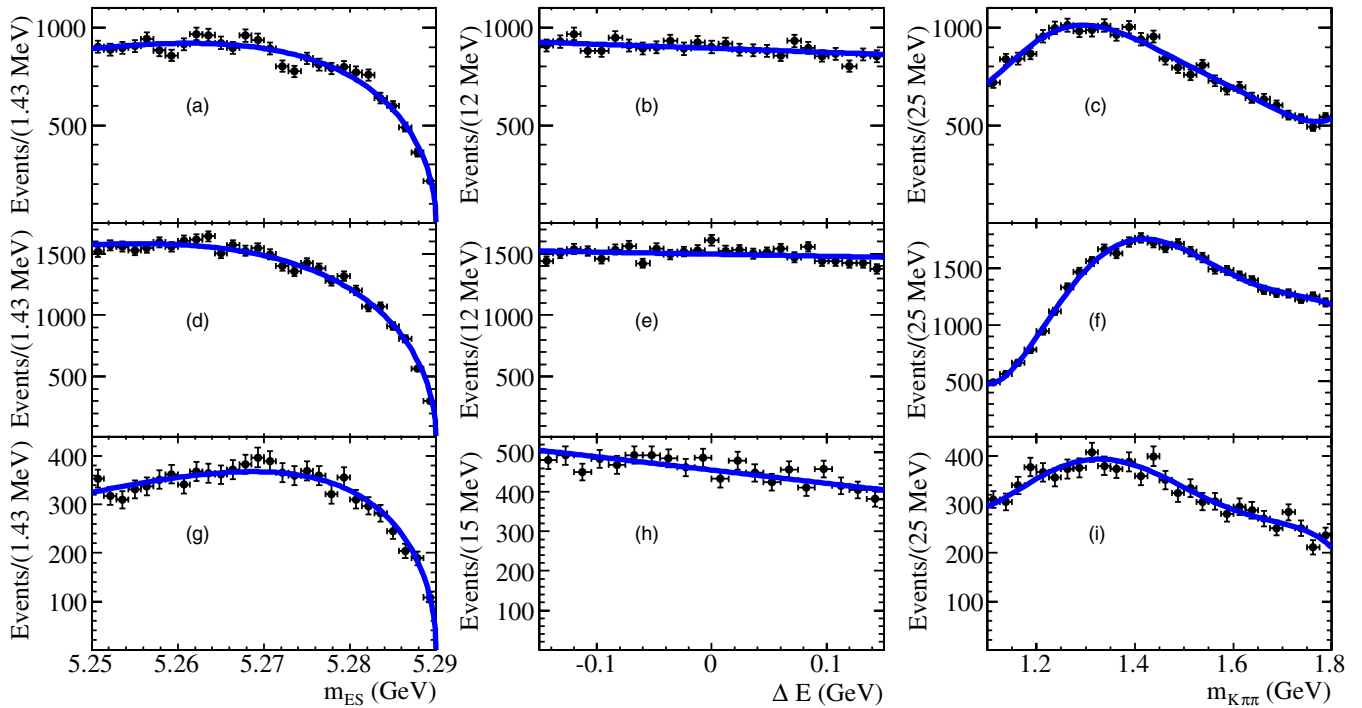

FIG. 4 (color online).   sPlot projections of combinatorial background onto m_{ES} (left), ΔE (center), and $m_{K\pi\pi}$ (right) for B^0 class 1 (top), B^0 class 2 (middle), and B^+ class 1 (bottom) events: the points show the sums of the combinatorial background weights obtained from on-resonance data. The solid line is the combinatorial background fit function. For $m_{K\pi\pi}$ the points are obtained without using information about resonances in the fit, i.e., we use only the m_{ES}, ΔE, and $\mathcal{F}$ variables.

TABLE III. Results of the ML fit at the absolute minimum of the $-\ln\mathcal{L}$ scan. The first two rows report the values of the production parameters (ϑ, ϕ) that maximize the likelihood. The third and fourth rows are the reconstruction efficiencies, including the daughter branching fractions, for class 1 and class 2 events. The fifth row is the correction for the fit bias to the signal branching fraction. The sixth row reports the results for the $B \to K_1(1270)\pi + K_1(1400)\pi$ branching fraction and its error (statistical only).

	$B^0 \to K_1^+ \pi^-$	$B^+ \to K_1^0 \pi^+$
ϑ	0.86	0.71
ϕ	1.26	3.14 (fixed)
ϵ_1 (%)	3.74	1.36
ϵ_2 (%)	1.68	$\cdots$
Fit bias correction ($\times 10^{-6}$)	$+0.0$	$+0.7$
$\mathcal{B}$ ($\times 10^{-6}$)	32.1 ± 2.4	22.8 ± 5.1

variables in which the projection variable is omitted. Using these weights, the data are then plotted as a function of the projection variable.

The results of the likelihood scans are shown in Table III and Fig. 5. At each point of the ζ scan the $-2\ln\mathcal{L}(\mathcal{B}; \zeta)$ function is minimized with respect to the signal branching fraction $\mathcal{B}$. Contours for the value $\mathcal{B}_{\max}(\zeta)$ that maximizes $\mathcal{L}(\mathcal{B}; \zeta)$ are shown in Figs. 5(c) and 5(d) as a function of the production parameters ζ, for B^0 and B^+ modes, respectively. The associated statistical error $\sigma_{\mathcal{B}}(\zeta)$ at each point ζ, given by the change in $\mathcal{B}$ when the quantity $-2\ln\mathcal{L}(\mathcal{B}; \zeta)$ increases by one unit, is displayed in Figs. 5(e) and 5(f). Systematics are included by convolving the experimental two-dimensional likelihood for ϑ and ϕ, $\mathcal{L} \equiv \mathcal{L}(\mathcal{B}_{\max}(\zeta); \zeta)$, with a two-dimensional Gaussian that accounts for the systematic uncertainties. In Figs. 6(a) and 6(b) we show the resulting distributions in ϑ and ϕ. The 68% and 90% probability regions are shown in dark and light shading, respectively, and are defined as the regions
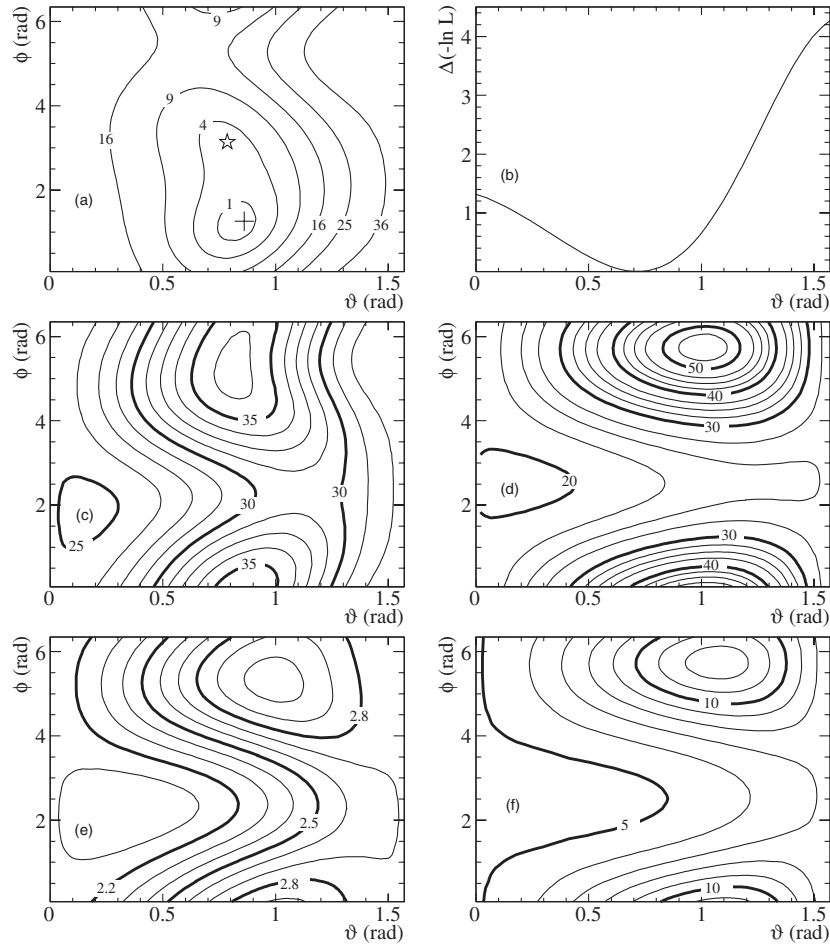

FIG. 5.   (a, b) $-\ln\mathcal{L}$ scan (systematics not included) in the production parameters ϑ and ϕ for the (a) B^0 and (b) B^+ modes. The cross in (a) indicates the position of the absolute minimum in the $-\ln\mathcal{L}$ scan. A second, local minimum is indicated by a star and corresponds to an increase in $\Delta(-\ln\mathcal{L})$ of 2.7 with respect to the absolute minimum. (c, d) Contours for the $B \to K_1(1270)\pi + K_1(1400)\pi$ branching fraction (in units of 10^{-6}) extracted from the ML fit for the (c) B^0 and (d) B^+ modes. (e, f) Contours for the statistical error (in units of 10^{-6}) on the $B \to K_1(1270)\pi + K_1(1400)\pi$ branching fraction for the (e) B^0 and (f) B^+ modes.
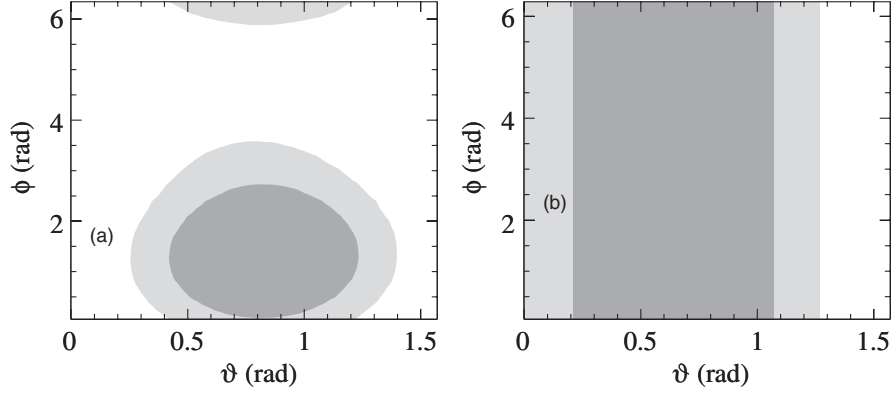
FIG. 6. (a, b) 68% (dark shaded zone) and 90% (light shaded zone) probability regions for ϑ and ϕ for the (a) B^0 and (b) B^+ modes.

consisting of all the points that satisfy the condition $\mathcal{L}(r) > x$, where the value x is such that $\int_{\mathcal{L}(r)>x} \mathcal{L}(\vartheta, \phi) d\vartheta d\phi = 68\%$ (90%). The significance is calculated from a likelihood ratio test $\Delta(-2\ln\mathcal{L})$ evaluated at the value of ϑ that maximizes the likelihood averaged over ϕ. Here $\Delta(-2\ln\mathcal{L})$ is the difference between the value of $-2\ln\mathcal{L}$ (convolved with systematic uncertainties) for zero signal and the value at its minimum for given values of ζ. We calculate the significance from a χ^2 distribution for $\Delta(-2\ln\mathcal{L})$ with 2 degrees of freedom. We observe nonzero $B^0 \to K_1^+\pi^-$ and $B^+ \to K_1^0\pi^+$ branching fractions with 7.5σ and 3.2σ significance, respectively.

We derive probability distributions for the $B \to K_1(1270)\pi + K_1(1400)\pi$, $B \to K_1(1270)\pi$, $B \to K_1(1400)\pi$, and $B \to K_{1A}\pi$ branching fractions.

At each point in the ζ plane we calculate the distributions for the branching fractions, given by $f(\mathcal{B}; \zeta) = c\mathcal{L}(\mathcal{B}; \zeta)$, where c is a normalization constant. Systematics are included by convolving the experimental one-dimensional likelihood $\mathcal{L}(\mathcal{B}; \zeta)$ with a Gaussian that represents systematic uncertainties. Branching fraction results are obtained by means of a weighted average of the branching fraction distributions defined above, with weights calculated from the experimental two-dimensional likelihood for ϑ and ϕ.

For each point of the ζ scan the $B \to K_1(1270)\pi$, $B \to K_1(1400)\pi$, and $B \to K_{1A}\pi$ branching fractions are obtained by applying ζ-dependent correction factors to the $B \to K_1(1270)\pi + K_1(1400)\pi$ branching fraction associated with that ζ point. The correction factor is calculated by reweighting the signal MC samples by setting the production parameters (f_{pa}, f_{pb}) equal to $(0, e^{i\phi}\sin\vartheta)$, $(\cos\vartheta, 0)$, and $(|f_{pA}|\cos\theta, -|f_{pA}|\sin\theta)$, for $B \to K_1(1270)\pi$, $B \to K_1(1400)\pi$, and $B \to K_{1A}\pi$, respectively, where $f_{pA} = \cos\vartheta \cos\theta - e^{i\phi}\sin\vartheta \sin\theta$ and θ is the K_1 mixing angle [19], for which we use the value $\theta = 72°$ (see Table I).

From the resulting distributions $f(\mathcal{B})$ we calculate the corresponding two-sided intervals at 68% probability, which consist of all the points $\mathcal{B} > 0$ that satisfy the condition $f(\mathcal{B}) > x$, where x is such that $\int_{f(\mathcal{B})>x, \mathcal{B}>0} f(\mathcal{B}) d\mathcal{B} = 68\%$. The upper limits (UL) at 90% probability are calculated as $\int_{0<\mathcal{B}<\mathrm{UL}} f(\mathcal{B}) d\mathcal{B} = 90\%$. The results are summarized in Table IV (statistical only) and Table V (including systematics).

We measure $\mathcal{B}(B^0 \to K_1(1270)^+\pi^- + K_1(1400)^+\pi^-) = 3.1^{+0.8}_{-0.7} \times 10^{-5}$ and $\mathcal{B}(B^+ \to K_1(1270)^0\pi^+ + K_1(1400)^0\pi^+) = 2.9^{+2.9}_{-1.7} \times 10^{-5}$ ($< 8.2 \times 10^{-5}$), where the two-sided ranges and upper limits are evaluated at 68% and 90% probability, respectively, and include systematic uncertainties.

TABLE IV. Branching fraction results for $B \to K_1\pi$ decays, in units of 10^{-5}, and corresponding confidence levels (C.L., statistical uncertainties only). For each branching fraction we provide the mean of the probability distribution, the most probable value (MPV), the two-sided interval at 68% probability, and the upper limit at 90% probability.

Channel	Mean	MPV	68% C.L. interval	90% C.L. UL
$B^0 \to K_1(1270)^+\pi^- + K_1(1400)^+\pi^-$	3.2	3.1	(2.9, 3.4)	3.5
$B^0 \to K_1(1270)^+\pi^-$	1.7	1.6	(1.3, 2.0)	2.1
$B^0 \to K_1(1400)^+\pi^-$	1.6	1.6	(1.3, 1.9)	2.0
$B^0 \to K_{1A}^+\pi^-$	1.5	1.4	(1.0, 1.9)	2.2
$B^+ \to K_1(1270)^0\pi^+ + K_1(1400)^0\pi^+$	2.9	2.3	(1.6, 3.5)	4.5
$B^+ \to K_1(1270)^0\pi^+$	1.1	0.3	(0.0, 1.4)	2.5
$B^+ \to K_1(1400)^0\pi^+$	1.8	1.7	(1.0, 2.5)	2.0
$B^+ \to K_{1A}^0\pi^+$	1.1	0.2	(0.0, 1.5)	2.3

TABLE V. Branching fraction results for $B \to K_1 \pi$ decays, in units of 10^{-5}, and corresponding confidence levels (C.L., systematic uncertainties included). For each branching fraction we provide the mean of the probability distribution, the most probable value (MPV), the two-sided interval at 68% probability, and the upper limit at 90% probability.

Channel	Mean	MPV	68% C.L. interval	90% C.L. UL
$B^0 \to K_1(1270)^+ \pi^- + K_1(1400)^+ \pi^-$	3.3	3.1	(2.4, 3.9)	4.3
$B^0 \to K_1(1270)^+ \pi^-$	1.7	1.7	(0.6, 2.5)	3.0
$B^0 \to K_1(1400)^+ \pi^-$	1.6	1.7	(0.8, 2.4)	2.7
$B^0 \to K_{1A}^+ \pi^-$	1.6	1.4	(0.4, 2.3)	2.9
$B^+ \to K_1(1270)^0 \pi^+ + K_1(1400)^0 \pi^+$	4.6	2.9	(1.2, 5.8)	8.2
$B^+ \to K_1(1270)^0 \pi^+$	1.7	0.0	(0.0, 2.1)	4.0
$B^+ \to K_1(1400)^0 \pi^+$	2.0	1.6	(0.0, 2.5)	3.9
$B^+ \to K_{1A}^0 \pi^+$	1.6	0.2	(0.0, 2.1)	3.6

Including systematic uncertainties we obtain the two-sided intervals (in units of 10^{-5}): $\mathcal{B}(B^0 \to K_1(1270)^+ \pi^-) \in [0.6, 2.5]$, $\mathcal{B}(B^0 \to K_1(1400)^+ \pi^-) \in [0.8, 2.4]$, $\mathcal{B}(B^0 \to K_{1A}^+ \pi^-) \in [0.4, 2.3]$, $\mathcal{B}(B^+ \to K_1(1270)^0 \pi^+) \in [0.0, 2.1]$ (< 4.0), $\mathcal{B}(B^+ \to K_1(1400)^0 \pi^+) \in [0.0, 2.5]$ (< 3.9), $\mathcal{B}(B^+ \to K_{1A}^0 \pi^+) \in [0.0, 2.1]$ (< 3.6), where the two-sided ranges and the upper limits are evaluated at 68% and 90% probability, respectively.

VIII. BOUNDS ON $|\Delta\alpha|$

We use the measurements presented in this work to derive bounds on the model uncertainty $|\Delta\alpha|$ on the weak phase α extracted in $B^0 \to a_1(1260)^\pm \pi^\mp$ decays. We use the previously measured branching fractions of $B^0 \to a_1(1260)^\pm \pi^\mp$, $B^0 \to a_1(1260)^- K^+$ and $B^+ \to a_1(1260)^+ K^0$ decays [4] and the CP-violation asymmetries [6] as input to the method of Ref. [8]. The values used are summarized in Tables VI and VII.

The bounds are calculated as the average of $|\Delta\alpha|^+ = |\alpha_{\text{eff}}^+ - \alpha|$ and $|\Delta\alpha|^- = |\alpha_{\text{eff}}^- - \alpha|$, which are obtained from the inversion of the relations [8]:

$$\cos 2(\alpha_{\text{eff}}^\pm - \alpha) \geq \frac{1 - 2R_\pm^0}{\sqrt{1 - \mathcal{A}_{CP}^{\pm 2}}},$$

$$\cos 2(\alpha_{\text{eff}}^\pm - \alpha) \geq \frac{1 - 2R_\pm^+}{\sqrt{1 - \mathcal{A}_{CP}^{\pm 2}}}, \qquad (24)$$

where we have defined the following ratios of CP-averaged rates [8]:

$$R_+^0 \equiv \frac{\bar{\lambda}^2 f_{a_1}^2 \bar{\mathcal{B}}(K_{1A}^+ \pi^-)}{f_{K_{1A}}^2 \bar{\mathcal{B}}(a_1^+ \pi^-)} \qquad R_-^0 \equiv \frac{\bar{\lambda}^2 f_\pi^2 \bar{\mathcal{B}}(a_1^- K^+)}{f_K^2 \bar{\mathcal{B}}(a_1^- \pi^+)}$$

$$R_+^+ \equiv \frac{\bar{\lambda}^2 f_{a_1}^2 \bar{\mathcal{B}}(K_{1A}^0 \pi^+)}{f_{K_{1A}}^2 \bar{\mathcal{B}}(a_1^+ \pi^-)} \qquad R_-^+ \equiv \frac{\bar{\lambda}^2 f_\pi^2 \bar{\mathcal{B}}(a_1^+ K^0)}{f_K^2 \bar{\mathcal{B}}(a_1^- \pi^+)}.$$

The CP asymmetries $\mathcal{A}_{CP}^\pm$ in $B^0 \to a_1^\pm \pi^\mp$ decays are related to the time- and flavor-integrated charge asymmetry $\mathcal{A}_{CP}^{a_1\pi}$ [6] by

$$\mathcal{A}_{CP}^+ = -\frac{\mathcal{A}_{CP}^{a_1\pi}(1 + \Delta C) + C}{1 + \mathcal{A}_{CP}^{a_1\pi} C + \Delta C},$$

$$\mathcal{A}_{CP}^- = \frac{\mathcal{A}_{CP}^{a_1\pi}(1 - \Delta C) - C}{1 - \mathcal{A}_{CP}^{a_1\pi} C - \Delta C}.$$

C and ΔC parametrize the flavor-dependent direct CP violation and the asymmetry between the CP-averaged rates $\bar{\mathcal{B}}(a_1^+ \pi^-)$ and $\bar{\mathcal{B}}(a_1^- \pi^+)$, respectively [8]:

$$C \pm \Delta C \equiv \frac{|A_\pm|^2 - |\bar{A}_\mp|^2}{|A_\pm|^2 + |\bar{A}_\mp|^2},$$

where the decay amplitudes for $B^0(\bar{B}^0) \to a_1(1260)^\pm \pi^\mp$ are

$$A_+ \equiv A(B^0 \to a_1^+ \pi^-), \qquad A_- \equiv A(B^0 \to a_1^- \pi^+),$$

$$\bar{A}_+ \equiv A(\bar{B}^0 \to a_1^- \pi^+), \qquad \bar{A}_- \equiv A(\bar{B}^0 \to a_1^+ \pi^-).$$

TABLE VI. Summary of the branching fractions used as input to the calculation of the bounds on $|\Delta\alpha|$ [4].

Decay mode	Branching fraction (in units of 10^{-6})
$B^0 \to a_1(1260)^\pm \pi^\mp$	$33.2 \pm 3.8 \pm 3.0$
$B^0 \to a_1(1260)^- K^+$	$16.3 \pm 2.9 \pm 2.3$
$B^+ \to a_1(1260)^+ K^0$	$33.2 \pm 5.0 \pm 4.4$

TABLE VII. Summary of the values of the CP-violation parameters used as input to the calculation of the bounds on $|\Delta\alpha|$ [6].

Quantity	Value
$\mathcal{A}_{CP}^{a_1\pi}$	$-0.07 \pm 0.07 \pm 0.02$
S	$0.37 \pm 0.21 \pm 0.07$
ΔS	$-0.14 \pm 0.21 \pm 0.06$
C	$-0.10 \pm 0.15 \pm 0.09$
ΔC	$0.26 \pm 0.15 \pm 0.07$

The CP-averaged rates are calculated as

$$\bar{\mathcal{B}}(a_1^+ \pi^-) = \frac{1}{2} \mathcal{B}(a_1^\pm \pi^\mp)(1 + \Delta C + \mathcal{A}_{CP}^{a_1\pi} C),$$

$$\bar{\mathcal{B}}(a_1^- \pi^+) = \frac{1}{2} \mathcal{B}(a_1^\pm \pi^\mp)(1 - \Delta C - \mathcal{A}_{CP}^{a_1\pi} C),$$

where $\mathcal{B}(a_1^\pm \pi^\mp)$ is the flavor-averaged branching fraction of neutral B decays to $a_1(1260)^\pm \pi^\mp$ [4].

For the constant $\bar{\lambda} = |V_{us}|/|V_{ud}| = |V_{cd}|/|V_{cs}|$ we take the value 0.23 [12]. The decay constants $f_K = 155.5 \pm 0.9$ MeV and $f_\pi = 130.4 \pm 0.2$ MeV [12] are experimentally known with small uncertainties. For the decay constants of the a_1 and K_{1A} mesons the values $f_{a_1} = 203 \pm 18$ MeV [31] and $f_{K_{1A}} = 207$ MeV [3] are used. For $f_{K_{1A}}$ we assume an uncertainty of 20 MeV. The value assumed for the $f_{K_{1A}}$ decay constant is based on a mixing angle $\theta = 58°$ [3], because $f_{K_{1A}}$ is not available for the value $\theta = 72°$ used here (see Table I); this discrepancy is likely accommodated within the accuracy of the present experimental constraints on the mixing angle. Using naïve arguments based on SU(3) relations and the mixing formulas, we have verified that the dependence of $f_{K_{1A}}$ on the mixing angle is rather mild in the θ range [58, 72]°. It should be noted that due to a different choice of notation, a positive mixing angle in the formalism used by the ACCMOR Collaboration [19] and in this paper corresponds to a negative mixing angle with the notation of Ref. [3].

We use a Monte Carlo technique to estimate a probability region for the bound on $|\alpha_{\text{eff}} - \alpha|$. All the CP-averaged rates and CP-violation parameters participating in the estimation of the bound are generated according to the experimental distributions, taking into account the statistical correlations among $\mathcal{A}_{CP}^{a_1\pi}$, C, and ΔC [28].

For each set of generated values we solve the system of inequalities in Eq. (24), which involve $|\alpha_{\text{eff}}^+ - \alpha|$ and $|\alpha_{\text{eff}}^- - \alpha|$, and calculate the bound on $|\alpha_{\text{eff}} - \alpha|$ from

$$|\alpha_{\text{eff}} - \alpha| \leq (|\alpha_{\text{eff}}^+ - \alpha| + |\alpha_{\text{eff}}^- - \alpha|)/2. \quad (25)$$

The probability regions are obtained by a counting method: we estimate the fraction of experiments with a value of the bound on $|\alpha_{\text{eff}} - \alpha|$ greater than a given value. We obtain $|\alpha_{\text{eff}} - \alpha| < 11°(13°)$ at 68% (90%) probability.

The determination of α_{eff} [6] presents an eightfold ambiguity in the range $[0°, 180°]$. The eight solutions are $\alpha_{\text{eff}} = (11 \pm 7)°$, $\alpha_{\text{eff}} = (41 \pm 7)°$, $\alpha_{\text{eff}} = (49 \pm 7)°$, $\alpha_{\text{eff}} = (79 \pm 7)°$, $\alpha_{\text{eff}} = (101 \pm 7)°$, $\alpha_{\text{eff}} = (131 \pm 7)°$, $\alpha_{\text{eff}} = (139 \pm 7)°$, $\alpha_{\text{eff}} = (169 \pm 7)°$ [6]. Assuming that the relative strong phase between the relevant tree amplitudes is negligible [8] it is possible to reduce this ambiguity to a twofold ambiguity in the range $[0°, 180°]$: $\alpha_{\text{eff}} = (11 \pm 7)°$, $\alpha_{\text{eff}} = (79 \pm 7)°$. We combine the solution near 90°, $\alpha_{\text{eff}} = (79 \pm 7)°$ [6], with the bounds on $|\alpha_{\text{eff}} - \alpha|$ and estimate the weak phase $\alpha = (79 \pm 7 \pm 11)°$. This solution is consistent with the current

average value of α, based on the analysis of $B \rightarrow \pi\pi$, $B \rightarrow \rho\rho$, and $B \rightarrow \rho\pi$ decays [12,32].

IX. SUMMARY

We present results from a branching fraction measurement of $B \rightarrow K_1(1270)\pi$ and $K_1(1400)\pi$ decays, obtained from a data sample of 454×10^6 $\Upsilon(4S) \rightarrow B\bar{B}$ events. The signal is modeled with a K-matrix formalism, which accounts for the effects of interference between the $K_1(1270)$ and $K_1(1400)$ mesons. Including systematic and model uncertainties, we measure $\mathcal{B}(B^0 \rightarrow K_1(1270)^+\pi^- + K_1(1400)^+\pi^-) = 3.1^{+0.8}_{-0.7} \times 10^{-5}$ and $\mathcal{B}(B^+ \rightarrow K_1(1270)^0\pi^+ + K_1(1400)^0\pi^+) = 2.9^{+2.9}_{-1.7} \times 10^{-5}$ ($< 8.2 \times 10^{-5}$ at 90% probability). A combined signal for the decays $B^0 \rightarrow K_1(1270)^+\pi^-$ and $B^0 \rightarrow K_1(1400)^+\pi^-$ is observed with a significance of 7.5σ, and the following branching fractions are derived for neutral B meson decays: $\mathcal{B}(B^0 \rightarrow K_1(1270)^+\pi^-) \in [0.6, 2.5] \times 10^{-5}$, $\mathcal{B}(B^0 \rightarrow K_1(1400)^+\pi^-) \in [0.8, 2.4] \times 10^{-5}$, and $\mathcal{B}(B^0 \rightarrow K_{1A}^+\pi^-) \in [0.4, 2.3] \times 10^{-5}$, where the two-sided intervals are evaluated at 68% probability. A significance of 3.2σ is obtained for $B^+ \rightarrow K_1(1270)^0\pi^+ + K_1(1400)^0\pi^+$, and we derive the following two-sided intervals at 68% probability and upper limits at 90% probability: $\mathcal{B}(B^+ \rightarrow K_1(1270)^0\pi^+) \in [0.0, 2.1] \times 10^{-5}$ ($< 4.0 \times 10^{-5}$), $\mathcal{B}(B^+ \rightarrow K_1(1400)^0\pi^+) \in [0.0, 2.5] \times 10^{-5}$ ($< 3.9 \times 10^{-5}$), and $\mathcal{B}(B^+ \rightarrow K_{1A}^0\pi^+) \in [0.0, 2.1] \times 10^{-5}$ ($< 3.6 \times 10^{-5}$).

Finally, we combine the results presented in this paper with existing experimental information to derive an independent estimate for the CKM angle α, based on the time-dependent analysis of CP-violating asymmetries in $B^0 \rightarrow a_1(1260)^\pm \pi^\mp$, and find $\alpha = (79 \pm 7 \pm 11)°$.

---

[1] V. Laporta, G. Nardulli, and T. N. Pham, Phys. Rev. D **74**, 054035 (2006); **76**, 079903(E) (2007).

[2] G. Calderon, J. H. Munoz, and C. E. Vera, Phys. Rev. D **76**, 094019 (2007).

[3] H.-Y. Cheng and K.-C. Yang, Phys. Rev. D **76**, 114020 (2007).

[4] B. Aubert *et al.* (*BABAR* Collaboration), Phys. Rev. Lett. **97**, 051802 (2006); **100**, 051803 (2008).

[5] B. Aubert *et al.* (*BABAR* Collaboration), Phys. Rev. Lett. **99**, 261801 (2007); **99**, 241803 (2007).

[6] B. Aubert *et al.* (*BABAR* Collaboration), Phys. Rev. Lett. **98**, 181803 (2007).

[7] N. Cabibbo, Phys. Rev. Lett. **10**, 531 (1963); M. Kobayashi and T. Maskawa, Prog. Theor. Phys. **49**, 652 (1973).

[8] M. Gronau and J. Zupan, Phys. Rev. D **73**, 057502 (2006); **70**, 074031 (2004).

[9] M. Gronau and J. L. Rosner, Phys. Lett. B **595**, 339 (2004).

[10] M. Beneke, M. Gronau, J. Rohrer, and M. Spranger, Phys. Lett. B **638**, 68 (2006).

[11] B. Aubert *et al.* (*BABAR* Collaboration), Phys. Rev. D **76**, 052007 (2007).

[12] C. Amsler *et al.* (Particle Data Group), Phys. Lett. B **667**, 1 (2008).

[13] Except as noted explicitly, we use a particle name to denote either member of a charge conjugate pair.

[14] H. Albrecht *et al.* (ARGUS Collaboration), Phys. Lett. B **254**, 288 (1991).

[15] K. Abe *et al.* (Belle Collaboration), Phys. Rev. Lett. **87**, 161601 (2001); H. Yang *et al.* (Belle Collaboration), Phys. Rev. Lett. **94**, 111802 (2005); B. Aubert *et al.* (*BABAR* Collaboration), Phys. Rev. Lett. **101**, 161801 (2008).

[16] B. Aubert *et al.* (*BABAR* Collaboration), Nucl. Instrum. Methods Phys. Res., Sect. A **479**, 1 (2002).

[17] G. Benelli *et al.*, *Nuclear Science Symposium Conference Record* (IEEE, New York, 2005), Vol. 2, p. 1145.

[18] S. Agostinelli *et al.*, Nucl. Instrum. Methods Phys. Res., Sect. A **506**, 250 (2003).

[19] C. Daum *et al.* (ACCMOR Collaboration), Nucl. Phys. **B187**, 1 (1981).

[20] I. J. R. Aitchison, Nucl. Phys. **A189**, 417 (1972).

[21] M. Nauenberg and A. Pais, Phys. Rev. **126**, 360 (1962).

[22] M. G. Bowler, M. A. V. Game, I. J. R. Aitchison, and J. B. Dainton, Nucl. Phys. **B97**, 227 (1975); C. Daum *et al.* (ACCMOR Collaboration), Nucl. Phys. **B182**, 269 (1981); M. G. Bowler, J. Phys. G **3**, 775 (1977); L. Stodolsky, Phys. Rev. Lett. **18**, 973 (1967); I. J. R. Aitchison and M. G. Bowler, J. Phys. G **3**, 1503 (1977).

[23] C. Daum *et al.* (ACCMOR Collaboration), Nucl. Phys. **B182**, 269 (1981).

[24] D. J. Herndon, P. Söding, and R. J. Cashmore, Phys. Rev. D **11**, 3165 (1975).

[25] R. L. Kelly *et al.* (Particle Data Group), Rev. Mod. Phys. **52**, S1 (1980).

[26] A. de Rújula, J. Ellis, E. G. Floratos, and M. K. Gaillard, Nucl. Phys. **B138**, 387 (1978).

[27] B. Aubert *et al.* (*BABAR* Collaboration), Phys. Rev. D **70**, 032006 (2004).

[28] E. Barberio *et al.* (Heavy Flavor Averaging Group), arXiv:0808.1297, and online update at http://www.slac.stanford.edu/xorg/hfag.

[29] H. Albrecht *et al.* (ARGUS Collaboration), Phys. Lett. B **241**, 278 (1990).

[30] M. Pivk and F. R. Le, Nucl. Instrum. Methods Phys. Res., Sect. A **555**, 356 (2005).

[31] J. C. R. Bloch, Yu. L. Kalinovsky, C. D. Roberts, and S. M. Schmidt, Phys. Rev. D **60**, 111502(R) (1999).

[32] J. Charles *et al.* (CKMFitter Group), Eur. Phys. J. C **41**, 1 (2005); M. Bona *et al.* (UTfit Collaboration), J. High Energy Phys. 03 (2006) 080.